Journal of Rock Mechanics and Geotechnical Engineering 16 (2024) 1000–1017

Contents lists available at ScienceDirect

Journal of Rock Mechanics and Geotechnical Engineering

journal homepage: www.jrmge.cn

Full Length Article

Dredged marine soil stabilization using magnesia cement augmented with biochar/slag

Chikezie Chimere Onyekwena [a,b], Qi Li [a,b,*], Yong Wang [a,b], Ishrat Hameed Alvi [a,b], Wentao Li [c], Yunlu Hou [a,b], Xianwei Zhang [a,d], Min Zhang [e,**]

[a] State Key Laboratory of Geomechanics and Geotechnical Engineering, Institute of Rock and Soil Mechanics, Chinese Academy of Sciences, Wuhan, 430071, China
[b] University of Chinese Academy of Sciences, Beijing, 100049, China
[c] School of Civil Engineering, Architecture and Environment, Hubei University of Technology, Wuhan, 430068, China
[d] School of Urban Construction, Wuhan University of Science and Technology, Wuhan, 430065, China
[e] School of Civil Engineering and Archtitecture, Henan University, Kaifeng, 475001, China

ARTICLE INFO

Article history:
Received 11 January 2023
Received in revised form
23 March 2023
Accepted 15 May 2023
Available online 30 June 2023

Keywords:
Dredged marine soil
CO_2 uptake
Reactive magnesia
Biochar
Ground granulated blast-furnace slag

ABSTRACT

Dredged marine soils (DMS) have poor engineering properties, which limit their usage in construction projects. This research examines the application of reactive magnesia (rMgO) containing supplementary cementitious materials (SCMs) to stabilize DMS under ambient and carbon dioxide (CO_2) curing conditions. Several proprietary experimental tests were conducted to investigate the stabilized DMS. Furthermore, the carbonation-induced mineralogical, thermal, and microstructural properties change of the samples were explored. The findings show that the compressive strength of the stabilized DMS fulfilled the 7-d requirement (0.7–2.1 MPa) for pavement and building foundations. Replacing rMgO with SCMs such as biochar or ground granulated blast-furnace slag (GGBS) altered the engineering properties and particle packing of the stabilized soils, thus influencing their performances. Biochar increased the porosity of the samples, facilitating higher CO_2 uptake and improved ductility, while GGBS decreased porosity and increased the dry density of the samples, resulting in higher strength. The addition of SCMs also enhanced the water retention capacity and modified the pH of the samples. Microstructural analysis revealed that the hydrated magnesium carbonates precipitated in the carbonated samples provided better cementation effects than brucite formed during rMgO hydration. Moreover, incorporating SCMs reduced the overall global warming potential and energy demand of the rMgO-based systems. The biochar mixes demonstrated lower toxicity and energy consumption. Ultimately, the rMgO and biochar blend can serve as an environmentally friendly additive for soft soil stabilization and permanent fixation of significant amounts of CO_2 in soils through mineral carbonation, potentially reducing environmental pollution while meeting urbanization needs.

1. Introduction

Marine soils, known as problematic and sensitive soils, are generally found in coastal regions, lowlands, offshore areas, and other parts of the earth. Dredging lakes, rivers, and estuaries is regularly performed to remove accumulated sediments and maintain navigation channels (Chan and Abdul Jalil, 2014). However, these dredged marine soils (DMS) usually end up as wastes (Lang et al., 2021a; Zhang et al., 2022). Moreover, there are strict regulations regarding the disposal of DMS waste on land or in the ocean due to the potential for environmental pollution and water contamination (Zhu et al., 2020). As a result, recycling DMS for construction purposes is a preferable solution that addresses both environmental concerns and the scarcity of land, especially when utilized for reclamation projects to meet the ever-burgeoning demand of the increasing population (Shi et al., 2017; Wu et al., 2022). Nevertheless, DMS presents various complexities, including high compressibility, swelling and shrinkage tendencies, low strength,

* Corresponding author. State Key Laboratory of Geomechanics and Geotechnical Engineering, Institute of Rock and Soil Mechanics, Chinese Academy of Sciences, Wuhan, 430071, China.
** Corresponding author.
E-mail addresses: qli@whrsm.ac.cn (Q. Li), minzhang@henu.edu.cn (M. Zhang).
Peer review under responsibility of Institute of Rock and Soil Mechanics, Chinese Academy of Sciences.

https://doi.org/10.1016/j.jrmge.2023.05.005

excessive settlement, and prolonged consolidation (Lang et al., 2021b; Onyekwena et al., 2023a). Consequently, the reuse of waste DMS as construction material poses a significant challenge for engineering geologists and geotechnical engineers due to its unfavorable engineering properties.

The Achilles heel of Portland cement (PC), commonly employed for recycling waste materials into reliable construction products, is the significant CO_2 emissions, high energy, and elevated temperatures involved in its production (Eyo et al., 2020; Lang et al., 2021b; Sharma et al., 2021; Alvi et al., 2023). Thus, alternative binders have been proposed to partially or fully replace the *P*C-based binder group. Among the various candidates, reactive magnesia (rMgO) has emerged as a sustainable binder mainly due to its high CO_2 sequestration capacity and the energy savings associated with the lower manufacturing temperatures (700–1000 °C) compared to the production temperature of PC (1450 °C) (Wu et al., 2018; Kara et al., 2021; Li et al., 2021). However, despite the promising nature of the rMgO binder, its production from magnesite releases chemical CO_2 similar to PC production, and the maximum absorbed CO_2 remains lower than the amount produced during its manufacture owing to current technology limitations and various influencing factors during carbonation (Grünhäuser Soares and Castro-Gomes, 2021; Onyekwena et al., 2023b). In addition, Shen et al. (2016) demonstrated that rMgO production emits more CO_2 than PC production and expressed concerns over the ability of rMgO to reabsorb CO_2 from the atmosphere. Hence, rMgO use should be moderated. Another challenge presented by the magnesia material group is its slow dissolution under ambient conditions, limiting its efficacy as a stabilization agent (Dung and Unluer, 2020).

CO_2 curing has emerged as a greener technique that employs carbon dioxide gas as a curing agent instead of the traditional steam and moisture, thus accelerating the curing process of cementitious materials and reducing their carbon footprint while enhancing strength and durability (Liu and Meng, 2021). However, the rapid reaction between rMgO and CO_2 results in the precipitation of bulk and expansive hydrated magnesium carbonates (HMCs) on the surface of rMgO particles, hindering further contact between CO_2 and fresh rMgO, thus leaving unreacted rMgO within the cementitious matrix, which presents an ineffective use of the rMgO binder as a stabilizer under CO_2 curing (Pu and Unluer, 2020). Nonetheless, adding supplementary cementitious materials (SCMs) into rMgO-based systems in different replacement ratios is reported to address this problem (Mo et al., 2017; Ruan et al., 2021).

The utilization of waste-derived products, such as ground granulated blast-furnace slag (GGBS), fly ash, and biochar, as SCMs for partial replacement of PC offers both environmental and economic benefits (Estabragh et al., 2020). Numerous studies (e.g. Zhang et al., 2020; Lang et al., 2021a; Li et al., 2022b) have explored the efficacy of GGBS as a cementitious material in solidifying dredged contaminated sediments or slurry. These investigations address the environmental concerns associated with contaminated sediments and emphasize the need to develop effective and sustainable solutions to mitigate their impact. Li et al. (2022a) and Zhang et al. (2022) also synthesized previous research on the mechanical behavior, leachability, and pH of GGBS-based solidified soils, highlighting the wide utilization of rMgO as an activator for GGBS. Estabragh et al. (2020) noted that GGBS alone may not achieve the desired performance as a stabilizing agent, but its effectiveness improves when activated by magnesia. According to Yi et al. (2014), the GGBS-rMgO blend demonstrated superior performance than the GGBS-lime blend based on the unconfined compressive strength (UCS) assessment. Wang et al. (2021) probed the role of biochar and CO_2 curing in rMgO paste and found that prewetted biochar acted as an internal curing source due to biochar's high water retention capability, which was beneficial in improving the mechanical performance. In recent years, biochar has gained attention as a climate change mitigator due to its carbon storage ability, leading to increased utilization in various applications. Biochar offers several advantages for geotechnical purposes, including water retention for hydration reactions, pH moderation to facilitate the required pozzolanic reactions, and increased cation supply. Studies (Dissanayake et al., 2020; He et al., 2021) demonstrate that in addition to its high affinity for CO_2 adsorption under ambient conditions, biochar can also absorb toxic metals and harmful gases (Sethupathi et al., 2017; Zhao et al., 2021). Several studies (e.g. Pardo et al., 2019; Reddy et al., 2020; Y. Zhang et al., 2020; Han et al., 2022) have reported that the addition of biochar improves the geotechnical properties of soil, such as elastic modulus, hydraulic properties, liquefaction resistance, shrinkage, and swelling properties. Onyekwena et al. (2022) investigated the performance of biochar-amended soil for engineered landfill applications and observed that biochar enhanced soil porosity under high compaction, enabling sufficient gas diffusion required for methane oxidation, root respiration, and plant growth. Although some studies (e.g. Wang et al., 2019a) have explored the impact of GGBS as SCM in carbonated rMgO-stabilized soil composites, the role of biochar in such systems remains unclear.

Therefore, to address this research gap, the main objective of this study is to investigate the functions of biochar or GGBS as supplementary cementitious materials admixed with rMgO for stabilizing dredged marine soil. To this end, equal proportions of rMgO-biochar/GGBS were chosen to assess the performance of stabilized DMS under ambient and CO_2 curing conditions. Furthermore, the environmental impact assessment and energy demand of the various mixes were evaluated.

2. Materials and methodology

2.1. Materials

The materials utilized in this study include DMS, rMgO, biochar, and GGBS. The waste DMS was dredged from Hangzhou Bay, situated at the intersection of the Qiantang River and the East China Sea (Fig. 1). To ensure experimental reproducibility and eliminate contaminants, the waste DMS was pre-treated by natural drying, grinding, and sieving (Yu et al., 2021). According to the unified soil classification system (ASTM D2487–11, 2011), the dredged marine soil was classified as a low plasticity silty clay (CL). The specific gravity of the DMS, determined following ASTM D854-10 (2010), was found to be 2.71. The compaction characteristics, including dry density and moisture content, were determined per ASTM D4609-08 (2008). The main binder used in this study is rMgO, sourced from Sinopharm Chemical Reagents Co., Ltd. Biochar and GGBS were acquired from a local supplier in Wuhan, China. The biochar used in the study is derived from the pyrolysis of wheat straw biomass.

The chemical compositions of the binders were analyzed using X-ray fluorescence (XRF), as shown in Table 1. The particle size distribution (PSD) of the rMgO, biochar, and GGBS determined using a laser particle size analyzer are shown in Fig. 2. The PSD of the natural soil was determined using the hydrometer method, with an average particle diameter (D50) calculated as 16 μm. The rMgO and GGBS particle diameters are finer than DMS and biochar.

2.2. Specimen preparation

In this study, a total binder content of 15% relative to the weight of waste DMS was employed, following the recommendation from a previous study by Cai et al. (2021) which suggested a suitable binder content of 15 wt% based on the mass of dry soil. The mix

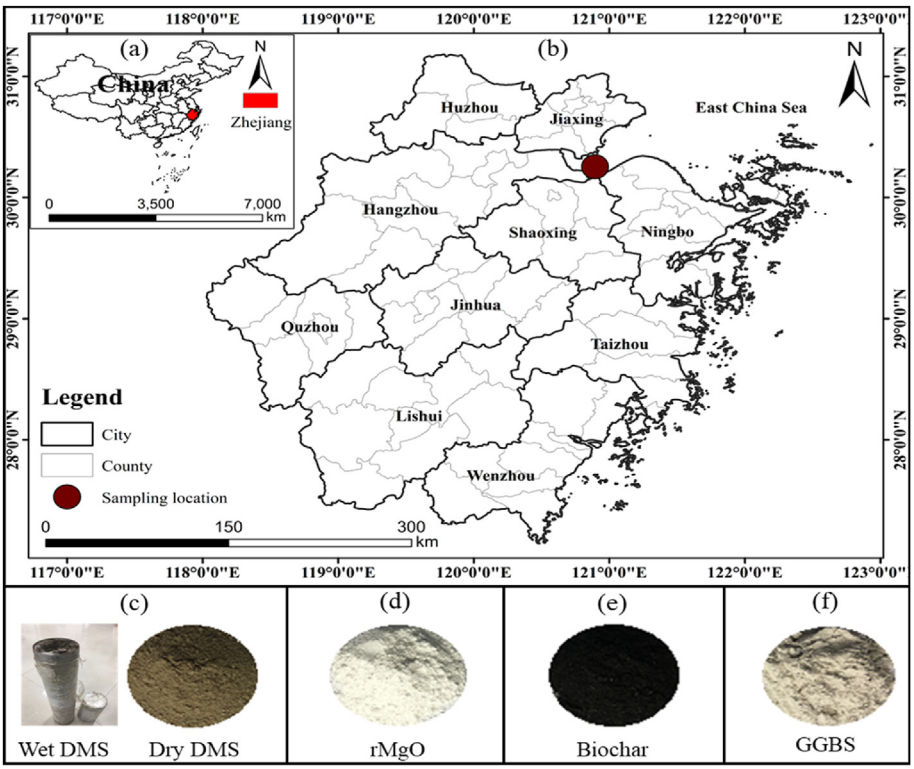

Fig. 1. Sampling location and materials: (a) China map, (b) Sampling location in Zhejiang Province, (c) Dredged marine soil, (d) Reactive magnesia, (e) Biochar, and (f) Ground granulated blast-furnace slag.

designs were determined based on preliminary tests, and the proportions of rMgO to biochar/GGBS are presented in Table 2. Equal replacement ratios of SCMs were selected to maintain consistency and differentiate the roles of SCMs in modifying the engineering properties of the rMgO mixes. Furthermore, the study aimed to utilize as much biochar and GGBS since using the waste-derived products in reasonable amounts will provide maximum benefit for circular economy and decarbonization strategies (Gonzalez et al., 2021).

The waste DMS was mixed with the additives and homogenized in a mixer for 5 min. Distilled water content obtained from compaction tests of the different samples (i.e. optimum moisture contents) was added to the homogenized mixture and stirred for another 5 min. The stabilized mixtures were allowed to mellow for 24 h and compacted to their maximum dry densities in a cylindrical mould (Φ50 mm × H100 mm) using a hydraulic jack (Wang et al., 2019b; Akula and Little, 2020; Cai et al., 2021). The samples were prepared in duplicates, sealed hermetically using plastic bags, and placed in a standard curing chamber (temperature: 20 ± 2 °C; relative humidity: 95%). Two curing conditions were adopted in this study: (1) The ambient cured samples were cured in the curing chamber for 7 d and 28 d; (2) The CO_2 cured samples were pre-conditioned for the first 24 h and then subjected to accelerated carbonation (CO_2 concentration: 99.9%, CO_2 pressure: 0.2 MPa) for 3 h, 6 h, and 12 h.

The curing periods (7 d and 28 d) for the ambient cured samples were selected based on the typical behavior of cement-admixed composites, which generally achieve 50%–70% of the required compressive strength at 7 d and 90%–95% at 28 d. At the same time, the curing periods for the CC samples were selected following previous study (Cai et al., 2021). Preconditioning was conducted to promote hydration reaction between water and rMgO grains essential for subsequent carbonation (Onyekwena et al., 2023b). In addition, water is consumed during the hydration process, paving the way for enhanced CO_2 diffusion during the carbonation stage (Liu and Meng, 2021). Since the carbonation curing is an exothermic process, the hot samples were mellowed for 12 h after the carbonation before conducting subsequent tests.

2.3. Carbonation setup

The apparatus shown in Fig. 3 was utilized to perform the carbonation experiment in this study. The self-developed carbonation apparatus was designed to withstand high pressures. In addition, the developed system is cost-effective, less time-consuming, more portable, and easier to handle than the modified triaxial apparatus (Yi et al., 2016; Wang et al., 2019b). The developed apparatus can operate without using water as hydrostatic or confining pressure, thus minimizing complexity and eliminating the risk of water intrusion during high-pressure carbonation. However, the classical triaxial apparatus may offer more precise testing and the ability to measure additional parameters.

The specimens were sealed on both ends of the moulds using stainless steel caps (Fig. 3). Porous stones were emplaced before sealing to prevent direct gas pressure on the wet specimen and to ensure uniform distribution of the CO_2 gas through the specimens. The CO_2 gas flow through the specimens was regulated by inflow and outflow valves. The whole system was vacuumed to remove free air before applying CO_2 gas. Before carbonation, the mass of the mould and the uncarbonated sample was recorded as an initial mass (m_o); after carbonation, the mass of the mould and the carbonated specimen was recorded as m_t. The mass of the mould and sample were measured using a high-precision digital balance with a readability of 0.01 g (Wang et al., 2019a), as shown in the experimental setup illustrated in Fig. 4. A pressure meter was

Table 1
Chemical composition of binders using X-ray fluorescence.

Chemical composition (%)	MgO	CaO	SiO_2	Fe_2O_3	Al_2O_3	K_2O_3	TiO_3	SO_3	LOI
Soil	1.6	0.57	69.78	4.611	17.21	3.4	0.93	0.11	1.79
rMgO	≥ 99	0.17	0.07	0.01	0.01	ND	ND	0.05	0.74
GGBS	6.94	46.58	26.36	0.41	15.16	0.42	0.75	2.72	0.65
Biochar	2.37	14.63	52.04	6	12.01	7.29	0.95	0.62	4

Note: ND: not detected, LOI: loss on ignition.

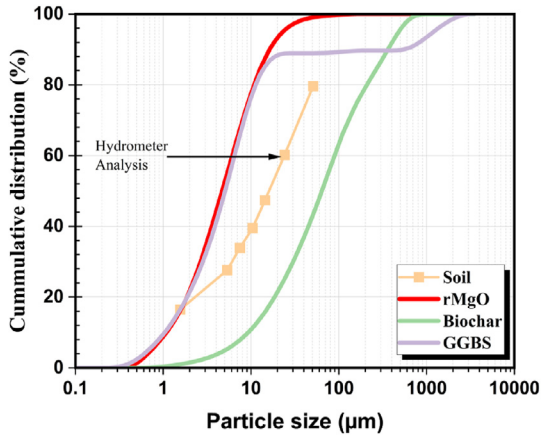

Fig. 2. Particle size distribution curves of the DMS, rMgO, biochar, and GGBS.

Table 2
Mix design and curing period for experiment samples.

Sample ID	Binder composition (%)			Curing period	
	rMgO	Biochar	GGBS	Ambient cured (d)	CO_2 cured (h)
M15	15	0	0	7, 28	3, 6, 12
M10-B5	10	5	0		
M7.5-B7.5	7.5	7.5	0		
M10-G5	10	0	5		
M7.5-G7.5	7.5	0	7.5		

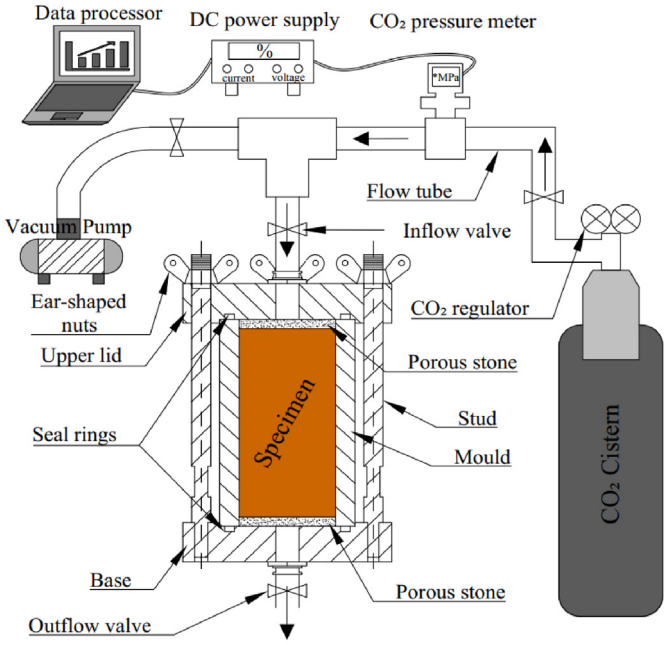

Fig. 3. Laboratory carbonation system setup.

employed to ensure consistent gas pressure, while a data processor connected to a power supply was used for data visualization. The sequestered CO_2 (g) measurement followed the methodology established in previous studies (Wang et al., 2019a; Li et al., 2021):

$$m_{co_2} = m_t - m_o \quad (1)$$

where m_{co_2} is the sequestered CO_2 in grams.

2.4. Testing methods

A series of laboratory experiments was conducted to assess the mechanical, physicochemical, and CO_2 uptake performances, including the microstructure and mineralogical properties of the stabilized waste DMS. All samples were subjected to UCS tests following ASTM D4219-08 (2008), and the strain rate was applied at 1%/min until failure (Wang et al., 2020; Cai et al., 2021). The performance of the mix designs was evaluated using statistical techniques such as the analysis of variance (ANOVA) and Fisher's least significant difference, with $P < 0.05$ regarded as statistically significant (Appendix A). The statistical analysis output is presented according to the performance and significance of the various mix designs for the applied curing periods and conditions. The moisture contents of the samples were measured, and the pH tests were performed using a pH meter, followed by microstructural and mineralogical tests to interpret changes in the intrinsic mechanism of the stabilized waste DMS. Some broken samples from the UCS tests were dried with a freeze-vacuum drier and subjected to microstructural and mineralogical analysis. The broken samples were deliberately selected from the midsection of the complete specimen to obtain a representative sample. One freeze-dried sample for each selected mix was coated with gold and used for the scanning electron microscopy (SEM) test. The remaining samples were crushed, ground, and sieved through a sieve with an aperture size of less than 0.075 mm. The resulting powder was subjected to X-ray diffraction (XRD) and thermogravimetric analysis (TGA) to identify the mineralogical and thermal properties. XRD patterns were obtained using a Bruker D8 X-ray diffractometer with a Cu kα source operating at 40 kV and 40 mA, scanning from 5° to 80° (2θ) at a rate of 2° (2θ/step). TGA testing was performed using a Mettler TGA/DSC instrument in a nitrogen gas environment at a heating rate of 10 °C/min from 40 °C to 1000 °C.

Fig. 4 shows the experimental routine, including the materials and mixing procedure, preliminary analysis, sample preparation, and major experimental explorations.

3. Results

3.1. Basic engineering characteristics

The soil consistency and the influence of additives on soil properties were evaluated based on the Atterberg limits. The addition of 15% rMgO resulted in a 33% increase in the liquid limit (LL), a 21% increase in the plastic limit (PL), and a 12% increase in the plasticity index (PI) compared to the natural soil (Fig. 5). rMgO has the ability to absorb water, undergo hydration, and precipitate brucite, which produces a porous matrix in the form of a flocculation blob (Cai et al., 2016). This process enhances the water demand of rMgO and its LL (Al-Tabbaa, 2013). Additionally, the rMgO additive reacts with clay particles, forming larger aggregates that improve soil structure and reduce water runoff.

Interestingly, replacing rMgO with biochar resulted in a further increase in the LL and a decrease in the PL compared to the M15 sample. The slight increase in LL observed with the incorporation of biochar can be attributed to its water-holding capacity (Choudhary

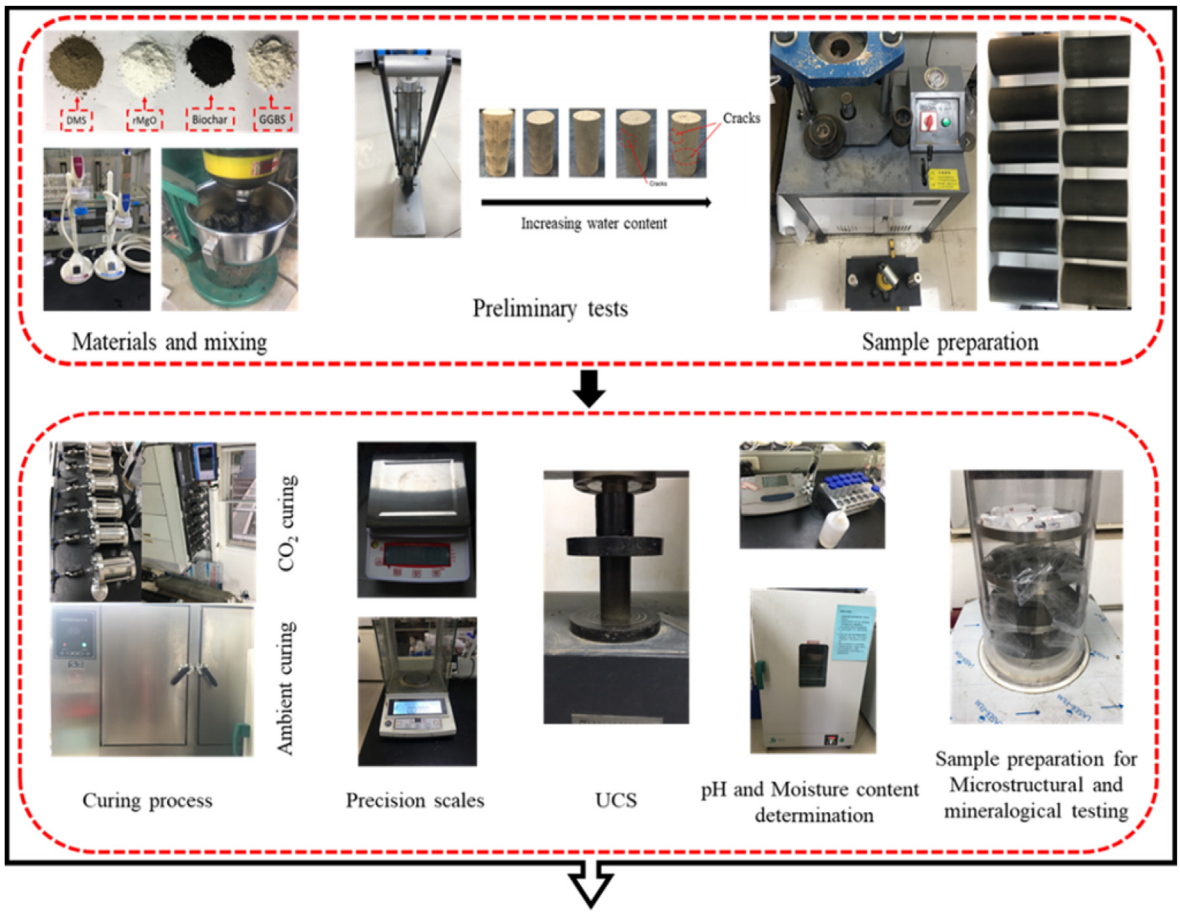

Fig. 4. Experimental procedure.

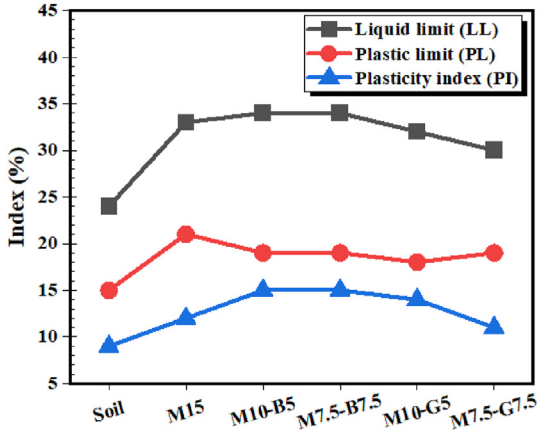

Fig. 5. Atterberg limits of the different mix designs.

et al., 2021). Moreover, this water-holding feature is beneficial for facilitating the precipitation of hydration products, as it ensures an adequate water supply for the hydration reaction, which is crucial for proper carbonation. Additionally, Choudhary et al. (2021) reported that the increased LL resulting from the addition of biochar could be ascribed to its high organic matter content, porosity, and surface area, which enable it to absorb and retain more water. The decrease in PL and the increase in the PI observed in the samples containing biochar aligns with the findings of Choudhary et al. (2021) regarding soil-biochar mixtures that do not contain rMgO.

On the contrary, the samples containing GGBS generally experienced a decrease in LL, PL, and PI (Sharma and Sivapullaiah, 2016; Geeta Rani et al., 2017). These observed reductions can be attributed to the flocculation of soil particles caused by the addition of GGBS. GGBS typically contains lime minerals (Noolu et al., 2021) with a significant CaO content (Table 1). When water and lime are added to clayey soil, the lime dissociates into Ca^{2+} and OH^{-} ions. The dissociated Ca^{2+} ions bond with the clay minerals, reducing repulsive forces and decreasing the thickness of the diffused water layer, bringing the soil particles closer. This process is known as flocculation and results in the formation of larger particle aggregates, increased water retention, and improved workability of soil (Manzoor and Yousuf, 2020).

The compaction graphs for the natural DMS and the rMgO mixes are presented in Fig. 6. Incorporating 15% rMgO resulted in a decrease in the dry densities (γ_d) and an increase in the water contents (W) of the stabilized DMS (i.e. soil-M15) due to the high water demand of rMgO (Al-Tabbaa, 2013). The addition of 5% and 7.5% biochar further contributed to the reduction in dry densities, likely due to the porous nature of biochar. In contrast, adding different percentages of GGBS led to an increase in dry densities and a decrease in the water contents of the rMgO-stabilized soils. The observed increase in dry densities with GGBS addition can be plausibly attributed to the fine particles of GGBS having a filler effect and causing flocculation of soil particles, resulting in the formation of dense agglomerate.

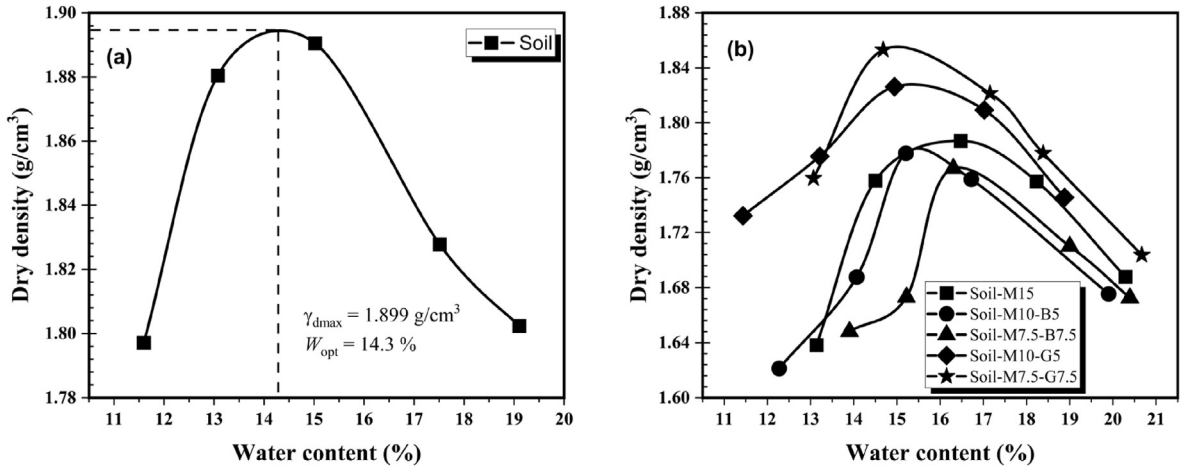

Fig. 6. Compaction graphs: (a) Natural DMS and (b) Different mix designs.

The basic engineering properties, including Atterberg limits, maximum dry densities, optimum water contents, void ratios, and porosities, of the natural and stabilized DMS are presented in Table 3. The addition of biochar increased the overall void ratios (e) and porosities (n) of the samples, while the addition of GGBS exhibited the opposite effect. The increase in void ratios and porosities in the biochar mixes can be attributed to the porous nature of biochar (Onyekwena et al., 2022). The void ratios and porosities were determined following standard phase relationships. The optimum water contents (W_{opt}) obtained from the compaction tests for each mix (Table 3) were utilized to prepare the soil samples to facilitate compaction that will achieve maximum dry densities (γ_{dmax}) of the samples before curing, as commonly practiced in soil stabilization (Yi et al., 2013; Yu et al., 2021).

Table 3
Summary of basic engineering properties.

Sample ID	LL (%)	PL (%)	PI (%)	γ_{dmax} (g/cm^3)	W_{opt} (%)	e	n (%)
Soil	24	15	9	1.89	14.3	0.43	29.93
M15	33	21	12	1.79	16.6	0.51	33.95
M10-B5	34	19	15	1.78	15.5	0.52	34.32
M7.5-B7.5	34	19	15	1.77	16.42	0.53	34.69
M10-G5	32	18	14	1.83	15.38	0.48	32.47
M7.5-G7.5	30	19	11	1.86	15	0.46	31.73

3.2. CO_2 uptake

The CO_2 uptake of the various samples, as estimated using Eq. (1), are illustrated in Fig. 7. Among the 3 h carbonated samples, the M10-B5 sample exhibited the highest CO_2 uptake. However, with extended carbonation up to 12 h, the M15 sample sequestered more CO_2 than the others. The increased CO_2 sequestration is attributed to the higher rMgO content in the M15 sample. Generally, the biochar mixes demonstrated a higher capacity for CO_2 sequestration compared to the GGBS samples. The enhanced CO_2 uptake capacity of the biochar samples can be ascribed to the high CO_2 adsorption capacity and porosity of biochar (Dissanayake et al., 2020; Onyekwena et al., 2022). This finding is supported by the results in Table 3, where the biochar samples exhibited the highest porosities and void ratios, facilitating CO_2 transport within the samples. Conversely, incorporating GGBS resulted in denser samples with fewer void spaces, leading to a reduction in the inflow of CO_2 gas.

The rMgO-CO_2 reaction sequence comprises rMgO hydration, CO_2 dissolution, and carbonation (Grünhäuser Soares and Castro-Gomes, 2021). rMgO reacts with water to form magnesium hydroxide, also known as brucite (Eq. (2)). During this process, the dissolution of rMgO releases Mg^{2+} into the pore fluid. When the concentration of Mg^{2+} and OH^- in the solution reaches a saturation threshold, they initiate nucleation and precipitate as $Mg(OH)_2$. The resulting brucite causes a considerable rise in pH, facilitating the dissolution of CO_2 in water to form carbonic acid. The carbonic acid reacts with the $Mg(OH)_2$/rMgO systems, generating carbonated products like magnesite or dense HMCs (such as nesquehonite, artinite, dypingite, and hydromagnesite). These carbonation products play a crucial role in enhancing the strength of carbonated rMgO composites. The hydration and carbonation products precipitate on the surface of rMgO particles, creating a physical barrier that hinders further interaction between water/CO_2 and fresh rMgO particles required for continuous hydration and carbonation reactions. As a result, carbonation efficiency decreases, impairing strength development (Pu and Unluer, 2020). However, under prolonged high-pressure exposure to carbonation, the brucite layer develops cracks due to volume expansion and exposes fresh unhydrated rMgO and uncarbonated brucite to react with the diffused CO_2 gas, leading to more CO_2 uptake and strength buildup. This phenomenon is illustrated in Fig. 7, where CO_2 uptake initially spikes in the first 3 h and gradually increases during subsequent

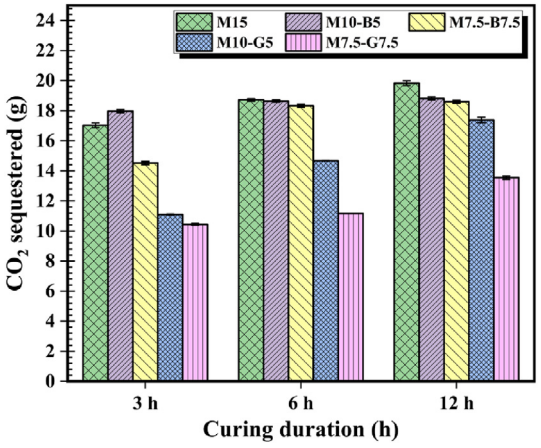

Fig. 7. CO_2 uptake of carbonated samples.

carbonation periods for the respective samples. The main hydration and carbonation products formed during the carbonation of rMgO composites are as follows (Unluer, 2018; Cai et al., 2020):

$$rMgO + H_2O \rightarrow Mg(OH)_2 \text{ (Brucite)} \quad (2)$$

$$Mg(OH)_2 + CO_2 + 2H_2O \rightarrow MgCO_3.3H_2O \text{ (Nesquehonite)} \quad (3)$$

$$5Mg(OH)_2 + 4CO_2 \rightarrow Mg_5(CO_3)_4(OH)_2.4H_2O \text{ (Hydromagnesite)} \quad (4)$$

$$5Mg(OH)_2 + 4CO_2 + H_2O \rightarrow Mg_5(CO_3)_4(OH)_2.5H_2O \text{ (Dypingite)} \quad (5)$$

It is noteworthy to mention that the degree of strength developed is contingent on the type of precipitated products, as elucidated in the following section.

3.3. Compressive strength

Fig. 8 presents the compressive strength. According to the Portland Cement Association (PCA) guide for cement-stabilized subgrade (CSS), the 7-d UCS values for pavement or building foundations typically range from 0.7 MPa to 2.1 MPa (100–300 psi) (Gross and Adaska, 2020). Fig. 8a shows that the unstabilized soil (DMS) has a relatively weak strength (0 MPa) even after 28 d curing. In comparison, the stabilized DMS samples surpassed the 7-d PCA strength requirement except for the M7.5-B7.5 samples falling between the upper and lower bounds of UCS (Fig. 8a). The CO_2 cured samples exhibit rapid strength gain within a short curing period (hours). At the same time, the ambient cured counterparts require longer curing periods (days). Furthermore, the UCS of CO_2 cured groups significantly surpassed the PCA requirement (Fig. 8b).

Compared to the CO_2 cured samples, the lower strength of the ambient cured samples can be attributed to the slow dissolution of rMgO under ambient conditions (Dung and Unluer, 2020). Additionally, the formation of brucite, which is the main hydration product formed in the ambient cured samples, exhibits lower binding ability compared to the HMCs precipitated in the CO_2 cured samples (Onyekwena et al., 2023b). Under the ambient cured and CO_2 cured conditions, rMgO effectively activated GGBS, resulting in higher strength performance. The higher strength of the GGBS samples is also attributed to the increased dry density caused by the filling effect of GGBS, as explained in section 3.1. Furthermore, the high CaO content from the XRF analysis is inclined to precipitate C–S–H during hydration and form calcite under carbonation curing, thus improving the strength of the samples. The enhanced performance of the CO_2 cured groups suggests that carbonation treatment utilizes sequestered CO_2 to enhance the mechanical performance of carbonated rMgO-stabilized DMS. Unlike energy-intensive and time-consuming steam and moisture curing methods (Liu and Meng, 2021), carbonation curing facilitates rapid strength gain in the stabilized soil samples. The UCS of the ambient cured samples increases with curing duration for various mix designs, while different strength development patterns are observed in the CO_2 cured groups with increasing carbonation periods. These distinct strength patterns in the CO_2 cured groups are linked to the hydration and carbonation mechanisms of the carbonated rMgO-cured samples and the precipitated products.

The CO_2 uptake of all carbonated samples increases with prolonged carbonation periods (Fig. 7). However, the UCS patterns vary, as shown in Fig. 8b, indicating that higher CO_2 uptake does not necessarily result in increased strength. Interestingly, the UCS of the M15 sample, carbonated for 3 h, decreases when subjected to 6 h carbonation curing. This can be attributed to the higher rMgO content in the M15 sample, which rapidly forms bulk and expansive hydration and carbonation products, inhibiting CO_2 gas diffusion into the cementitious matrix at greater depths. The precipitated carbonates expand under long-period high-pressure exposure to carbonation, inducing microcracks and weakening the strength. Nevertheless, as carbonation proceeds, unhydrated rMgO and uncarbonated hydration products are exposed through the cracks, allowing further reaction with diffused CO_2 to form additional carbonates. This results in strength buildup and increased CO_2 uptake, as observed in the 12 h carbonated M15 sample, which shows a slight strength increase following the initial decrease during the 6 h carbonation period (Fig. 8b).

Cai et al. (2021) reported that effective carbonation of plain rMgO-admixed silt with maximum strength was achieved in the first 3 h and that prolonged exposure to high-pressure conditions (>3 h) weakened the particle cementation and adversely affected the strength of the carbonated specimens. Our study further demonstrated that rMgO-stabilized soils containing SCMs like biochar or GGBS achieved effective carbonation with maximum strength within the first 6 h. This is attributed to the modification of sample porosity and particle packing by the SCMs, which induce delayed formation of expansive HMCs due to reduced rMgO content, enabling longer carbonation periods. However, beyond the 6 h carbonation period under high-pressure exposure, the strengths of the samples containing SCMs were affected. This suggests that the carbonation reaction is an expansive process linked to the reaction mechanism of rMgO-based systems during CO_2 curing.

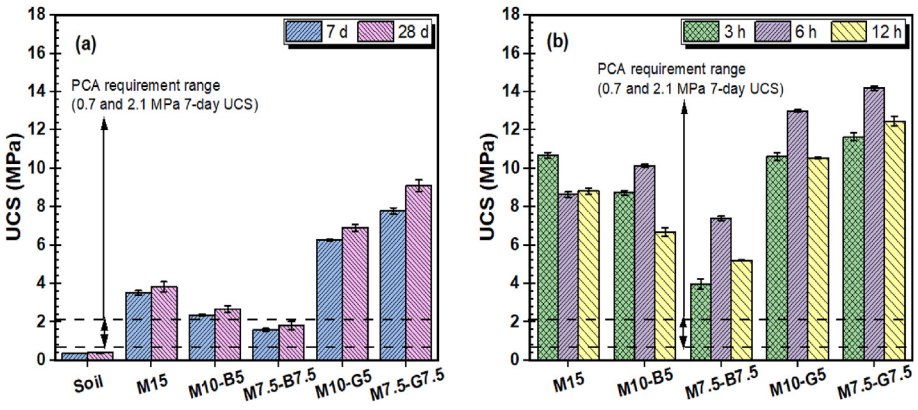

Fig. 8. Compressive strength of samples: (a) Ambient cured, and (b) CO_2 cured.

The crystalline magnesium carbonates formed in the CO_2 cured samples can saturate and precipitate in various sizes and shapes, continuously reforming under prolonged exposure to carbonation. In contrast, the ambient cured samples precipitate hydration products such as M-S-H, which possess silica networks in the form of sheet-like structures. These structures fill pore spaces more effectively and at lower saturation levels than carbonates. This may explain the consistent strength patterns observed in the ambient cured groups subjected to long-period curing compared to the CO_2 cured groups. Therefore, a 6 h carbonation period is recommended for effective carbonation of rMgO-stabilized soils containing SCMs under high-pressure exposure.

3.4. Stress-strain relationships

The stress-strain curves depicting the performance of different mix designs under various curing conditions and periods are presented in Fig. 9. The peaks of the curves correspond to the strain at failure, representing the UCS values. Generally, the CO_2 cured

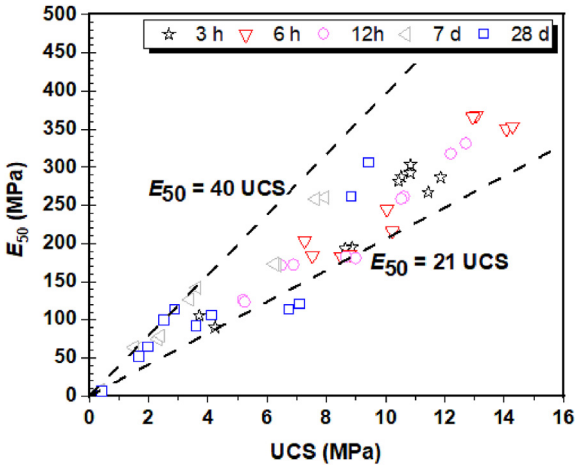

Fig. 10. Relationship between E_{50} and UCS of rMgO stabilized DMS.

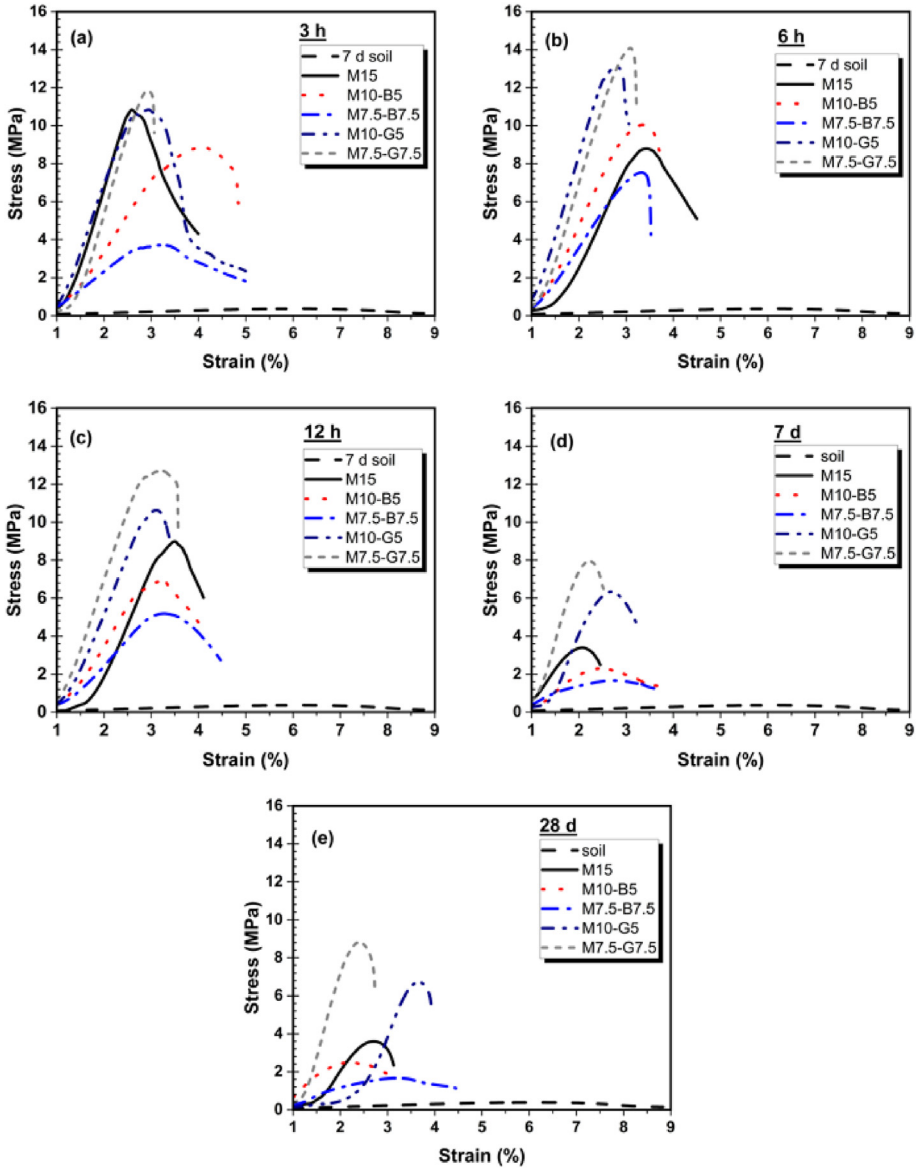

Fig. 9. Stress-strain relationship for the different mixes: (a)–(c) CO_2 cured, and (d)–(e) Ambient cured.

samples exhibited higher stress-strain curves than the ambient cured samples. This can be attributed to the carbonation reaction between CO_2 and hydration products, resulting in the precipitation of stable carbonates (Eqs. (3)–(5)), thereby improving the mechanical performance. Fig. 9a displays the stress-strain curves for 3 h carbonated samples. The lower curves of the biochar mixes can be attributed to the brittle and porous nature of biochar, which may deform under applied load. However, the addition of biochar generally enhanced the ductility of the samples compared to the rMgO-GGBS and plain rMgO samples, which exhibited greater stiffness and rigidity.

3.5. Deformation modulus

The correlation between the UCS and deformation modulus (E_{50}) of the stabilized DMS is presented in Fig. 10. The deformation modulus, also referred to as the secant modulus, was determined based on the stress-strain relationships at 50% of the maximum strength (Wang et al., 2016; Yaghoubi et al., 2018). In Fig. 10, a linear relationship is observed between E_{50} and UCS, which can be expressed as $E_{50} = \eta$UCS, where η is a dimensionless parameter (Du et al., 2013).

The E_{50} is an essential input parameter for analyzing the deformation behavior of treated soils (Cai and Liu, 2017), and the estimated correlation can be valuable for deriving the stiffness from strength when performing numerical simulations. Generally, the E_{50} increased with higher strength levels. Fig. 10 shows that the rMgO replacement level, the curing mode, and duration significantly influenced E_{50}. The 3-h and 6-h carbonated specimens exhibited higher deformation capabilities compared to other curing periods. In this study, the relationship between E_{50} and UCS for 15% rMgO-biochar/GGBS stabilized DMS can be expressed as $E_{50} = (21 - 40)$UCS. Previous research findings in Table 4 indicate that the deformation behavior of the 15% rMgO-biochar/GGBS stabilized DMS is similar to that of specimens stabilized with other binder materials.

3.6. Moisture content and pH

Fig. 11 illustrates the moisture content variations of the different samples under the ambient cured (Fig. 11a) and CO_2 cured (Fig. 11b) conditions. The untreated soil exhibited minimal moisture loss even after 28 dof curing (Fig. 11a) since there was no incorporated binder to react with water. In contrast, the addition of stabilizing agents led to significant water loss, with the CO_2 cured samples (Fig. 11b) consuming more water than the ambient cured samples. The higher water consumption in the CO_2 cured samples can be attributed to the exothermic reaction between rMgO and CO_2 during the carbonation process. The ambient cured samples, however, only consumed water during the hydration reaction (Cai et al., 2021). Notably, M15 had the highest water loss for both curing conditions, primarily due to the high water demand of rMgO (Al-Tabbaa, 2013). The replacement of rMgO with supplementary cementitious materials (SCMs) reduced the water demand of rMgO, which is advantageous for long-term hydration and pozzolanic reactions. Furthermore, M7.5-B7.5 demonstrated the highest water-holding capacity for both curing conditions, owing to the water retention ability of biochar.

Fig. 12 depicts the pH changes observed in the ambient and CO_2 cured samples. The inclusion of rMgO-biochar/GGBS increased the pH of the stabilized DMS. These pH variations were influenced by different processes, including the dissolution of rMgO-biochar/GGBS in an alkaline environment and the hydration and carbonation reactions. The former led to an increase in pH, while the latter contributed to a decrease in pH (Han et al., 2022). In general, the pH values of all samples decreased as the curing periods increased for both ambient and CO_2 cured conditions. However, the pH values of the CO_2 cured samples were lower than those of the ambient cured samples, which is attributed to the fact that the carbonation reaction is fundamentally an acid-alkaline neutralization reaction mechanism that consumes hydroxyl and magnesium ions, thereby depleting the pH in the pore solution. Conversely, the pH of the untreated soil barely changed after 7 d and 28 d of ambient curing due to the absence of additives to modify the pH.

The pH values of the rMgO-GGBS samples were higher (11.85–12.17) compared to other ambient-cured samples (10.5). The lime in the GGBS additive dissociates, generating OH^- ions, causing a rise in the pH value, consequently releasing and dissolving silica and alumina components from the clay mineral (Manzoor and Yousuf, 2020). These compounds interact with the calcium ions produced during hydration, forming cementitious hydrates such as C–S–H and C-A-H (Lang et al., 2021b). The elevated pH environment in the rMgO-GGBS samples likely contributed to the higher strength development since the mixtures were alkali enough for long-term pozzolanic reactions (Gonzalez et al., 2021). Furthermore, the elevated pH values due to GGBS can help maintain the stability of hydration products in the stabilized DMS (Han et al., 2022).

Similarly, the high pH environment in the rMgO-GGBS samples may have contributed to the strength development in the CO_2 cured groups, as observed by the significant drop in pH under carbonation curing conditions. The 3 h carbonated samples had higher pH values than the 6 h and 12 h samples. However, pH values decreased significantly with long-period high-pressure exposure to CO_2. Besides, the 6 h carbonated samples, which showed the highest strength for most samples, had lower pH values than the 12 h carbonated samples. This may result from the consumption of more hydroxyl ions during the carbonation reaction. The slight increase in pH of the 12 h carbonated specimens could be due to the formation of HMCs, which hinders further CO_2 diffusion into the mixture and enable the gradual dissolution of unreacted rMgO grains and uncarbonated $Mg(OH)_2$, thereby increasing the pH of the samples.

3.7. Microstructural and mineralogical analysis

This section presents the mineralogical and microstructural results of the selected samples, focusing on the 6 h and 28 d cured samples, which exhibited the best performance under their respective curing regimes. Understanding the mineralogical and microstructural characteristics is crucial for gaining insights into the reaction mechanism of rMgO-stabilized DMS.

Fig. 13 presents the XRD diffractograms of the selected samples. Fig. 13a shows the XRD patterns of the ambient cured samples. The predominant minerals identified in the unstabilized DMS were quartz, primarily composed of silica (SiO_2), balipholite ($BaLiMg_2Al_3(Si_2O_6)_2(OH)_4$) (Ma and Han, 1987), and gismondine ($Ca_2Al_4Si_4O_{16}.9H_2O$) (Ma et al., 2023). The low CaO and MgO content in the natural soil (Table 1) suggests a limited amount of reactive components available for CO_2 reaction. However, these identified

Table 4
E_{50} and UCS relationship for different percentage binders and materials.

Material	Relationship	Source
Zinc-polluted soil with cement (12%–18%)	$E_{50} = (18 - 53)$UCS	Du et al. (2013)
Silt soil with reactive MgO (5%–30%)	$E_{50} = (30 - 200)$UCS	Cai and Liu (2017)
DMS with reactive MgO-biochar/GGBS (15%)	$E_{50} = (21 - 40)$UCS	Present work

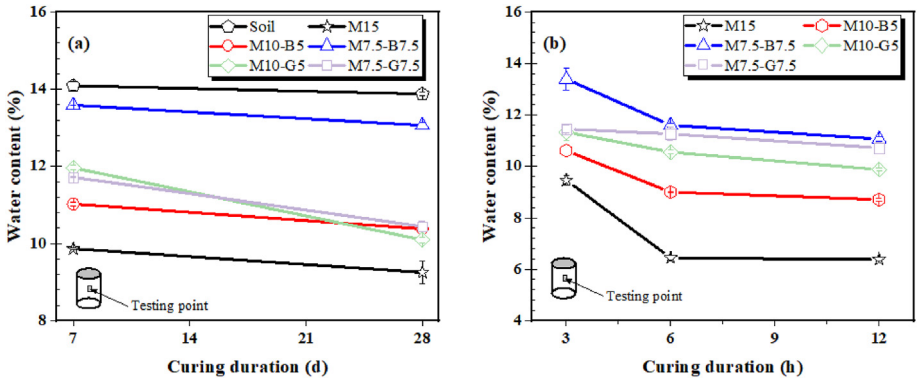

Fig. 11. Average moisture content of all samples: (a) Ambient cured, and (b) CO_2 cured.

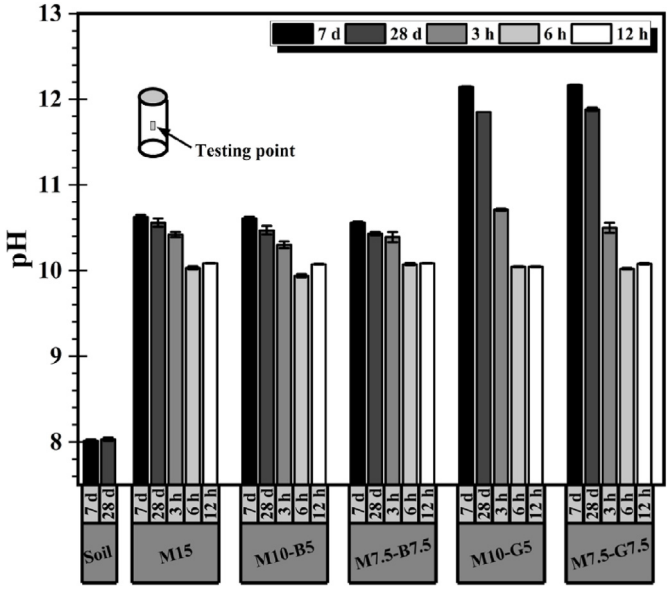

Fig. 12. Average pH of Ambient cured (7 d and 28 d) and CO_2 cured (3 h, 6 h, and 12 h) samples.

elements can react with MgO in the presence of water during hydration to precipitate M-S-H and C–S–H gels (Lang et al., 2021b), which are, in part, with brucite, the main hydration products identified in the ambient cured samples of the rMgO-biochar/GGBS-stabilized DMS. Minor peaks corresponding to magnesium and calcium silicate hydrates were also detected (Fig. 13a). In the carbonated samples (Fig. 13b), the main hydrated magnesium carbonate phases identified were nesquehonite, hydromagnesite, and dypingite (Eqs. (3)–(5)). Small peaks of brucite were observed in the carbonated samples, which could explain the slight increase in UCS for M15 carbonated up to 12 h. This observation suggests that fresh, uncarbonated brucite exposed through cracks reacts with diffused CO_2 gas to form additional carbonates.

The M7.5-G7.5 had carbonate peaks with lower intensities, but the strength was not compromised, as shown in Fig. 8. This can be attributed to the formations of amorphous magnesium-calcium silicate hydrates and calcite, identified in the M7.5-G7.5 sample due to CaO within the GGBS binder. The occurrence of these phases, along with the high pH of the M7.5-G7.5 mix, could have contributed to its strength development (Ruan et al., 2021). Furthermore, the fine particle sizes of GGBS acted as a filler material, reducing the porosity of the specimen and densifying the sample during its reaction in a CO_2-rich environment, thus compensating for the

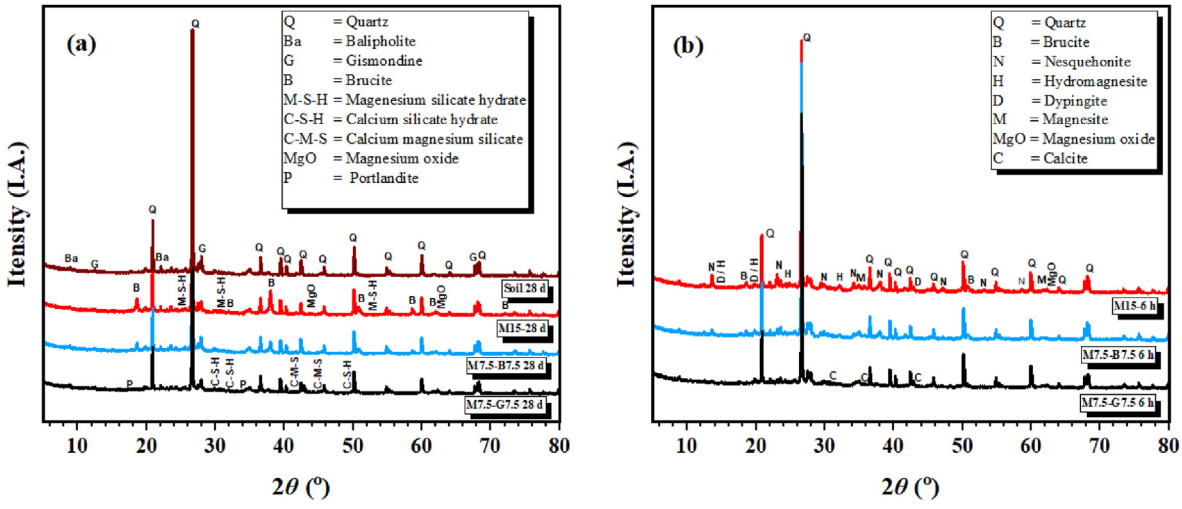

Fig. 13. XRD patterns of the selected samples: (a) Ambient cured amd (b) CO_2 cured.

reduced amount of precipitated HMCs. This filler effect of GGBS may have restrained the diffusion of CO_2 gas (Fig. 7), resulting in lower carbonation efficiency (Ruan et al., 2021) compared to the M7.5-B7.5 sample.

The TGA results in Fig. 14 depict the weight losses of the samples at varying temperatures. The CO_2 cured samples (Fig. 14b) exhibited significantly higher weight losses compared to the ambient cured samples (Fig. 14a). This is due to the formation of bulk HMCs and hydration products, resulting in higher strength development than the ambient cured samples which mainly consist of hydration products. According to previous studies (Dung and Unluer, 2017; Ruan and Unluer, 2017; Hay and Celik, 2020; Liu et al., 2020), three primary stages of decomposition were identified in the carbonated samples: (i) dehydration of water bonded to HMCs and hydration products occurring between (40–320) °C; (ii) dehydroxylation of HMCs, C–S–H and M-S-H gels and decomposition of uncarbonated $Mg(OH)_2$ and $Ca(OH)_2$ between (320–480) °C, indicating that the hydration products formed in the stabilized soil were not completely carbonated; (iii) decarbonation of HMCs between (480–1000) °C.

In Fig. 14a, dehydration of M-S-H and C–S–H gels was observed at 40–200 °C (Li et al., 2021), and the decompositions of $Mg(OH)_2$ and $Ca(OH)_2$ occurred at about (320–480) °C (Ruan and Unluer, 2017), while the peak at (400–500) °C can be attributed to the decomposition of organic matter in the DMS (Li et al., 2021). It is worth noting that the decomposition peaks related to M-S-H and C–S–H gels are attributed to the reaction between MgO, CaO, and SiO_2, contributed partly by the soil and biochar or GGBS additives (Table 1). Although additional constituents in the raw materials could impact the peak decomposition, their impact is negligible compared to the amount of magnesium and calcium carbonates precipitated through the carbonation of MgO-stabilized soils (Liu et al., 2020). Fig. 14a indicates that the weight loss of the M7.5-G7.5 sample was slightly higher than that of the M7.5-B7.5 counterpart. However, for the carbonated sample, the M7.5-B7.5 exhibited a higher weight loss compared to the M7.5-G7.5 (Fig. 14b). The total mass losses up to 1000 °C by TGA and UCS of the different samples after 6 h carbonation are presented in Fig. 15. It is worth mentioning that the mass losses due to the decarbonation of HMCs correspond to CO_2 uptake. The M10-B5 sample showed the highest weight loss, surpassing the M15 sample with higher rMgO content. This observation can explain the higher strength of the M10-B5 sample compared to the M15 sample after 6 h carbonation. Fig. 14b shows that from approximately 480 °C–1000 °C, the weight of the M10-B5 sample exceeded that of the M15 sample. Decarbonation of HMCs occurs within this temperature range,

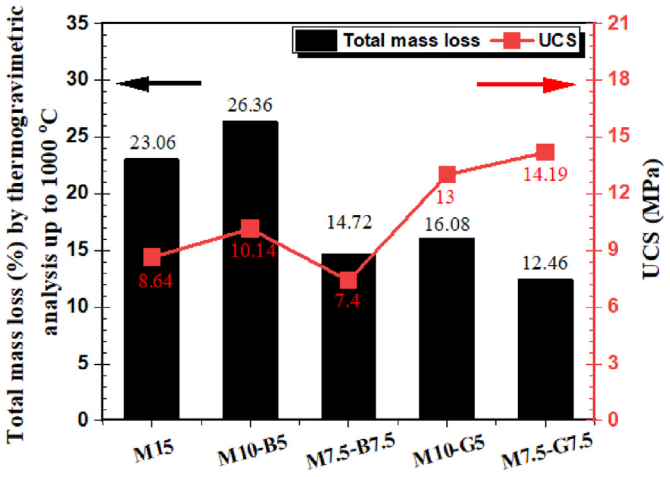

Fig. 15. Total mass loss (by thermogravimetric analysis up to 1000 °C) and UCS of selected samples after 6 h curing period.

indicating that the higher weight loss results from a higher carbonation degree.

Based on previous research (Ruan and Unluer, 2017; Liu et al., 2020), it has been established that the mass loss occurring between 480 °C and 1000 °C can be primarily attributed to the decomposition of magnesium and calcium carbonates. Consequently, this enables the feasibility of estimating CO_2 uptake efficiency (CO_{2eff}), referred to as method II in this study. The CO_2 uptake from the TGA analysis can be calculated using Eq. (6) (El-Hassan et al., 2013; Wang et al., 2019a; Gupta, 2021):

$$CO_{2eff}(\%) = \frac{(M_{480} - M_{1000})}{M_b} \times 100 \tag{6}$$

where M_{480} and M_{1000} are the mass of samples at 480 °C and 1000 °C, respectively, and M_b is the mass of the binder in the sample at 1000 °C. Furthermore, the theoretical maximum CO_2 uptake, based on total available Mg^{2+} and Ca^{2+}, can be calculated using Steinour's formula (Gupta, 2021; Ruan et al., 2021):

$$CO_{2th} = 0.785(CaO - 0.7SO_3) + 1.091MgO + 1.420Na_2O + 0.935k_2O \tag{7}$$

where CO_{2th} is the theoretical CO_2 uptake. Therefore, the CO_{2eff} can be written as

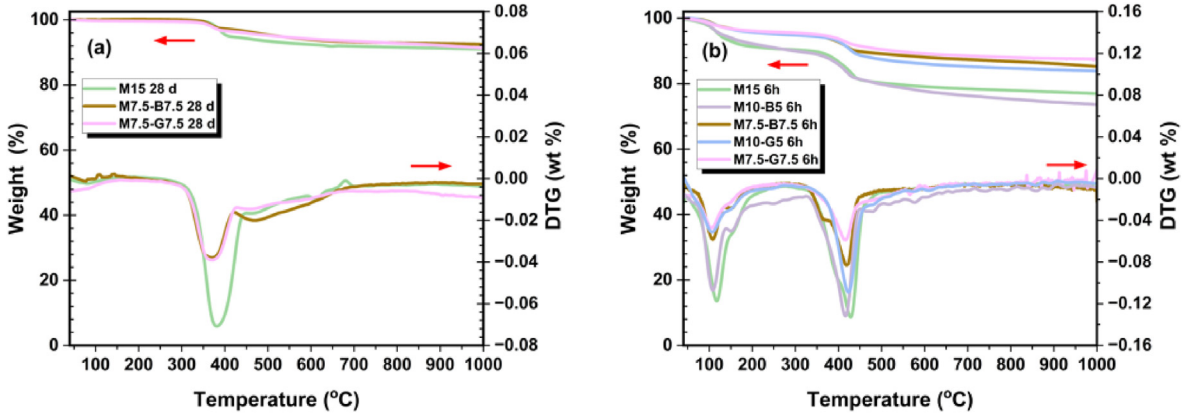

Fig. 14. TGA results of the selected samples: (a) Ambient cured and (b) CO_2 cured.

$$CO_{2eff}\ (\%) = \frac{m_{co_2}}{CO_{2th}} \times 100 \quad (8)$$

where m_{co_2} is the sequestered CO_2 (Fig. 7). The terms m_{co_2} and CO_{2th} denote the carbon capture determined theoretically and experimentally through mineralization. This approach enables the prediction of the CO_2 uptake capacity of binding materials and evaluates their efficiency in capturing CO_2 under specific carbonation conditions (Wang et al., 2019a).

Table 5 presents the weight losses at different temperature ranges and the calculated CO_2 uptake efficiencies using methods I and II. Interestingly, the CO_2 uptake efficiencies obtained from methods I and II are similar for most samples, except for M10-B5 and M7.5-B7.5. It is notable that dividing the sequestered CO_2 (i.e. m_{co_2}) by CO_{2th} yields higher CO_2 uptake efficiency for the M10-B5 and M7.5-B7.5 samples, as shown in Table 5. This observation suggests that estimates obtained using method I may be biased since biochar contains less MgO and CaO (Table 1), and substituting rMgO with biochar or GGBS reduces the availability of Mg^{2+} required for the precipitation of $MgCO_3$, resulting in lower theoretical CO_2 uptake. Wang et al. (2019a) demonstrated that CO_2 uptake efficiencies determined from TGA results are more reliable than the weight gain method, which is prone to experimental errors. The CO_2 uptake efficiencies calculated using method II (Table 5) indicate that 5 wt% replacement with biochar and GGBS facilitated higher CO_2 uptake than the M15 sample. It is apparent that the M15 sample, with a higher rMgO content, experienced a more rapid reaction with H_2O and CO_2, forming higher hydration products compared to the M10-B5 and M10-G5 samples. This is supported by the higher weight loss of hydration products at (320–480) °C and lower weight loss of carbonation products at (480–1000) °C observed in the M15 samples compared to the M10-B5 and M10-G5 samples. These findings indicate that most of the weight gained by the M15 sample is attributed to the precipitation of hydration products. The higher rMgO content in the M15 sample promoted the formation of a surface-layer coating of hydration products on the particles of rMgO, impeding gas diffusion and ultimately reducing the CO_2 uptake capacity of the sample during prolonged carbonation. The results from Wang et al. (2019a) demonstrate that the 24 h carbonated samples containing GGBS exhibit lower CO_2 uptake capacity than samples containing fly ash under both calculation methods (Table 5).

Incorporating 5 wt% biochar facilitated enhanced CO_2 gas diffusion and reactions with rMgO particles, resulting in higher carbonate precipitation compared to other samples. Fig. 16 shows the porous biochar within the biochar samples, which was not observed in plain rMgO or rMgO-GGBS samples. Therefore, biochar facilitated a high compaction degree while enabling sufficient inflow of CO_2 gas (Onyekwena et al., 2022). However, increasing the biochar content to 7.5 wt% (i.e. M7.5-B7.5) led to a reduction in CO_2 uptake due to the lower reactivity of the material in reacting with diffused CO_2, as the rMgO content is significantly reduced. Also, the improved water-retention capacity of the M7.5-B7.5 sample resulting from the higher biochar content may impede the flow of CO_2 gas through the pores.

Generally, while the biochar samples exhibited higher CO_2 uptake, the GGBS samples demonstrated higher strength. This distinction can be ascribed to the different roles of additives in the samples. Biochar enhanced the CO_2 sequestration capability by increasing the porosity of the samples, facilitating efficient CO_2 diffusion. Conversely, GGBS acted as a filler material, occupying pore spaces and densifying the sample structure, thereby improving strength but compromising the CO_2 uptake capacity. Based on these findings, rMgO replacements with 5 wt% biochar or GGBS is the most promising mixture for achieving desirable mechanical and CO_2 uptake performances. rMgO replacement with 5 wt% biochar reduced the rMgO content while improving the CO_2 sequestration capacity of the rMgO-stabilized soil.

Fig. 17 displays SEM images showcasing the microstructural evolution between the ambient and CO_2 cured samples. Various carbonates, notably the needle-like nesquehonite (N) and the rosette-flaky crystals of hydromagnesite/dypingite (D/H) were observed in all the carbonated rMgO-biochar/GGBS stabilized DMS samples (Fig. 17b, d, f), which are consistent with previous studies on carbonation of rMgO-treated soils (Cai et al., 2021; Wang et al., 2019b). The main hydration products observed in the ambient cured samples (Fig. 17a, c, e) are brucite, M-S-H, and C–S–H (Estabragh et al., 2020) except for the 28-d M7.5-G7.5 (Fig. 17e), which showed a small presence of portlandite, in agreement with Yi et al. (2014). Additionally, calcite was formed in the carbonated M7.5-G7.5 sample. Carbonate precipitation in the CO_2 cured samples contributed significantly to the strength development. The 6 h carbonated M7.5-B7.5 sample (Fig. 17d) showed higher nesquehonite precipitation compared to the 6 h carbonated M7.5-G7.5 sample (Fig. 17f), indicating a higher formation of HMCs within the M7.5-B7.5 sample. On the other hand, the GGBS samples (Fig. 17e

Table 5
Weight losses and calculated CO_2 uptake efficiencies using methods I and II (weight %).

Method	Mix label	Weight loss (wt.%) at 6 h			CO_{2eff} (II) (%)	m_{co_2} (g) at 6 h	CO_{2th} (g)	CO_{2eff} (I) (%)
		(40–320) °C	(320–480) °C	(480–1000) °C				
CO_2 uptake by TGA (Method II in this study)	M15	9.84	9.6	3.62	31.38	–	–	–
	M10-B5	10.36	9.21	6.79	61.49	–	–	–
	M7.5-B7.5	4.76	5.83	4.13	32.3	–	–	–
	M10-G5	5.28	6.83	3.97	31.52	–	–	–
	M7.5-G7.5	4.61	4.53	3.32	25.31	–	–	–
Wang et al. (2019a)	20P6F0L4MC				60.6–73.1			
Curing period: 24 h;	20P6S0L4MC				48.2–55.8			
Pressure: 0.15 MPa	20P6S1L3MC				30.8–34.5			
CO_2 uptake by Weight gain (Method I in this study)	M15	–	–	–	–	18.72	56.99	32.84
	M10-B5	–	–	–	–	18.65	41.38	45.06
	M7.5-B7.5	–	–	–	–	18.34	33.54	54.66
	M10-G5	–	–	–	–	14.67	46.59	31.49
	M7.5-G7.5	–	–	–	–	11.16	41.17	27.09
Wang et al. (2019a)	20P6F0L4MC							66–79.7
Curing period: 24 h;	20P6S0L4MC							58.1–67.5
Pressure: 0.15 MPa	20P6S1L3MC							56.1–63.3

P = percentage, F = fly ash, S = slag, L = lime, M = MgO, C = carbonated.

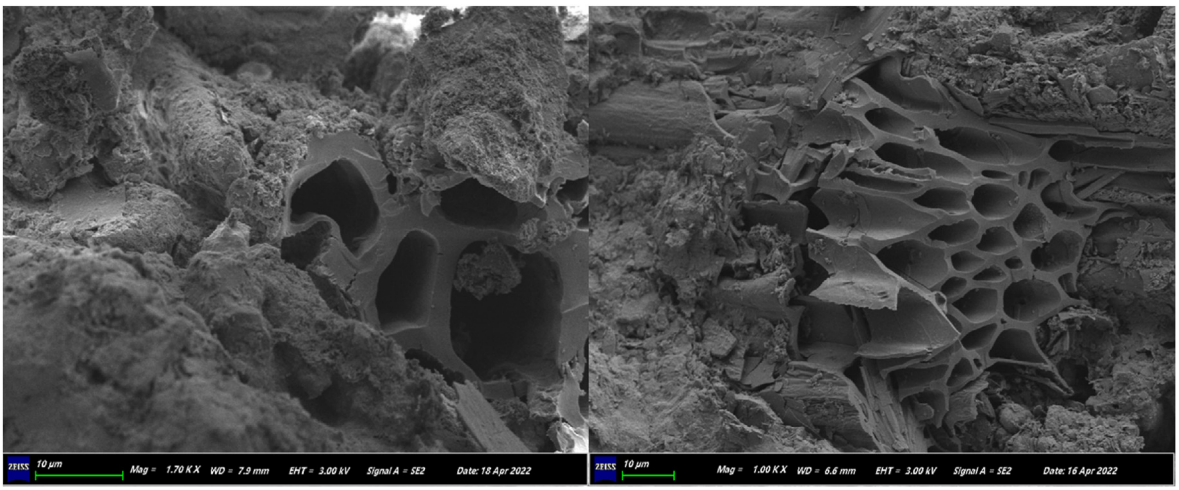

Fig. 16. SEM images showing porous biochar.

and f) had fewer pores than the biochar mixes (Fig. 17c and d) due to the fine particles of GGBS, which densified the microstructure. Cracks were observed in the 6 h carbonated M15 sample (Fig. 17b), which may explain the decrease in strength as a result of higher rMgO content present in the sample leading to the rapid formation of HMCs, which developed micro-cracks under long-period high-pressure carbonation, as explained in Section 3.3. The bulky HMCs and uncarbonated hydration products form on the surface of the rMgO grains, hindering CO_2 diffusion. However, with longer carbonation under a high-pressure CO_2 environment, fresh rMgO particles are exposed through the micro-cracks developed on the precipitated HMCs and react with diffused CO_2 gas, leading to more CO_2 uptake. Adding SCMs delayed the formation of HMCs due to reduced rMgO content, thus enabling longer carbonation (6 h) without developing micro-cracks.

From the SEM images, it can be inferred that HMCs exhibit better cementation effects than brucite, as evidenced by the superior mechanical performance of the CO_2 cured groups.

4. Discussion

Similar to PC production, the synthesis of rMgO from magnesite also emits carbon dioxide due to the chemical CO_2 associated with its parent raw material ($MgCO_3$) and the use of fossil fuels during manufacturing. However, previous studies, such as Wang et al. (2019b), have demonstrated that rMgO has a higher CO_2 sequestration ability than PC or lime and that its overall environmental burdens are lower. It is reported that the production of 1 kg of rMgO emits 1.1 kg of CO_2 (Ruan et al., 2020). Therefore, the use of rMgO should be controlled. Additionally, excessive rMgO content can pose challenges in controlling the expansion rate and induced cracks during carbonation, which may negatively impact the mechanical performance of carbonated rMgO samples. High rMgO content can affect carbonation efficiency in two ways: firstly, the rapid precipitation of hydration products and HMCs hinders CO_2 diffusion as carbonation progresses, and secondly, the fine particles of rMgO can act as fillers to inhibit CO_2 gas diffusion into the samples. Moreover, the high-water demand of rMgO binder restricts the availability of sufficient water for hydration and carbonation reactions when used excessively. Consequently, excess use of rMgO binder will increase its environmental impacts and impair the carbonation processes, ultimately compromising the strength of carbonated rMgO composites, which presents an inefficient use of the rMgO binder.

The environmental impacts associated with the production of additives are of great importance to decision-makers when selecting the type of SCMs for soil stabilization. Thus, an environmental impact assessment of rMgO-biochar/GGBS systems was performed to identify the more environment-friendly SCM for stabilizing dredged marine soil. Although there are several processes for producing rMgO in practice, the present study assumed that the rMgO was obtained from the calcination of magnesite:

$$MgCO_3 \rightarrow MgO + CO_2 \tag{9}$$

Fig. 18 illustrates the environmental impact assessment of the stabilized DMS. This section considered 1 tonne of stabilized DMS as a functional unit. The figure demonstrates that replacing rMgO with SCMs significantly reduced the global warming potential (GWP) of the rMgO-stabilized DMS. Replacing rMgO with 5 wt% biochar or GGBS resulted in a 32% decrease in GWP for the rMgO systems. However, rMgO replacement with GGBS increased the ecotoxicity of the samples (i.e. human, fresh water, and marine aquatic), while biochar addition reduced the toxicity of the samples. This indicates that the rMgO-biochar samples are less environmentally toxic compared to the plain rMgO and rMgO-GGBS samples. Furthermore, rMgO replacements with SCMs significantly reduced the eutrophication potential of the rMgO systems. Nevertheless, biochar was more effective in reducing the eutrophication of the rMgO-stabilized DMS. Therefore, biochar can be considered a more environmentally benign SCM for stabilizing waste DMS than GGBS. The energy consumption of the M15 sample was compared to that of the M10-B5 and M10-G5 samples. The input coefficients used for evaluation are presented in Table 6, and the cumulative energy demands (CED) of raw materials per tonne of stabilized DMS were estimated by

$$CED = \sum_{i=1}^{N} W_i \cdot IED^i \tag{10}$$

where N is the raw material type; W_i is the weight per unit of raw materials i; and IED^i is the individual energy demand per unit of raw materials used to produce 1 tonne of stabilized soil.

The energy consumption of the different raw materials is presented in Fig. 19. It is evident that rMgO constituted the majority of the energy consumption. rMgO replacement with 5 wt% biochar resulted in a decrease in energy consumption by 196.6 MJ/t, corresponding to a 27.9% reduction compared to the plain rMgO.

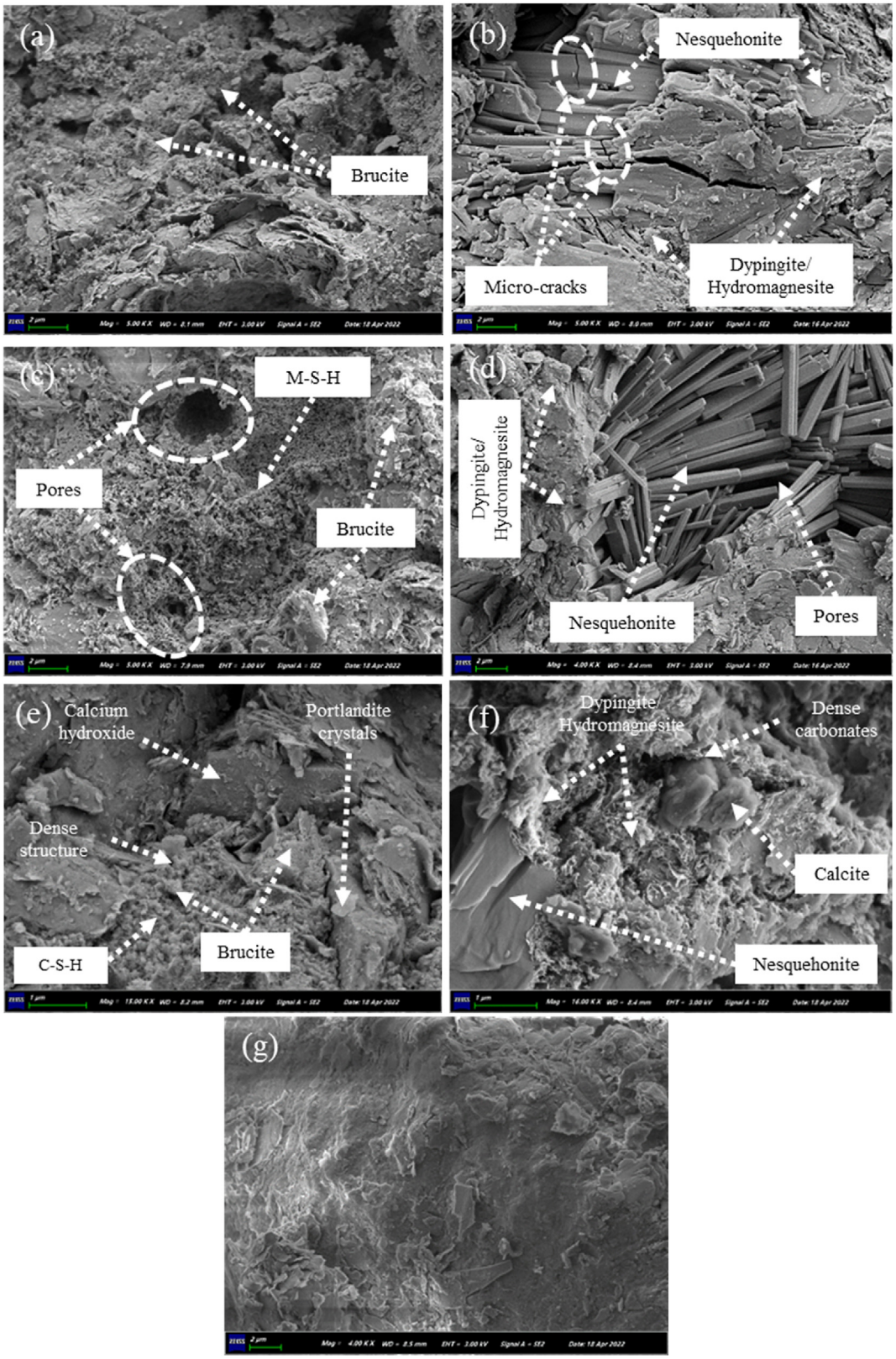

Fig. 17. SEM results for selected samples: (a) M15 of 28-d curing, (b) M15 of 6-h curing, (c) M7.5-B7.5 of 28-d curing, (d) M7.5-B7.5 of 6-h curing, (e) M7.5-G7.5 of 28-d curing, (f) M7.5-G7.5 of 6-h curing, and (g) Unstabilized soil of 28-d curing.

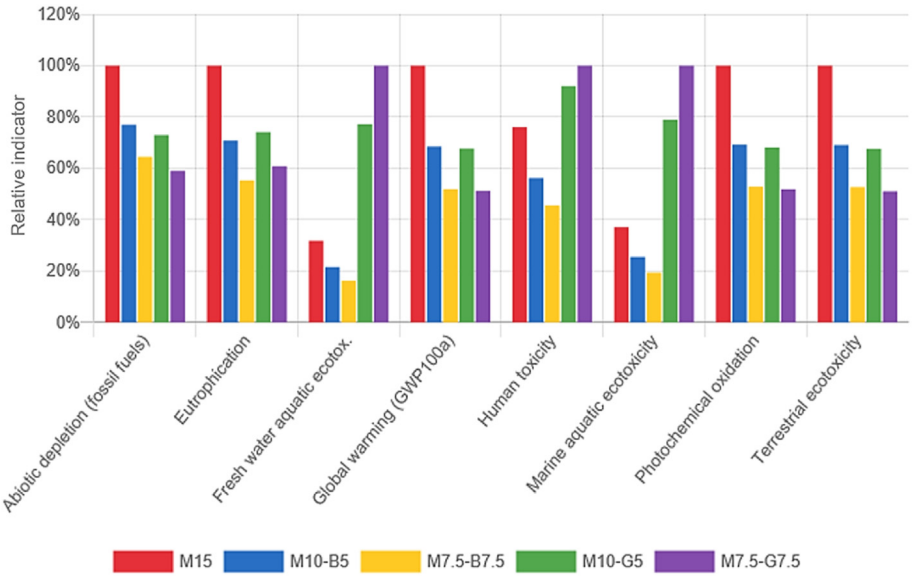

Fig. 18. Environmental impact assessment of the various mixes.

Similarly, rMgO replacement with 5 wt% GGBS led to a decrease in energy consumption by 178.1 MJ/t, corresponding to a 25.3% reduction compared to the plain rMgO sample. Therefore, biochar was more effective in reducing the energy demand of the stabilized DMS than GGBS.

Based on the microstructural analysis and the CO_2 uptake assessments, Fig. 20 illustrates the schematic representations of the possible interactions between CO_2, H_2O, soil, and the incorporated additives, along with the phase formation mechanisms of the various mixes after 6 h carbonation. The natural soil comprises quartz, balipholite, and gismondine as the main mineral phases (Fig. 14), and these minerals contain substantial silica and alumina content. Additionally, the significant presence of SiO_2 and Al_2O_3 in biochar and GGBS makes them viable candidates as pozzolanic materials capable of improving the soil. Hence, high magnesium (Mg) in the rMgO adsorbent can facilitate the dissolution of Si and Al in the amorphous soil and biochar/GGBS, creating an ideal environment for an effective pozzolanic reaction that produces alumina-silica-hydrate (A-S-H) gel (Fasihnikoutalab et al., 2017). The precipitated A-S-H gel then reacts with available Ca to form calcium aluminosilicate hydrate (C-A-S-H) gel. The chemical reactions involving Mg in the rMgO with silica or alumina are exemplified in Eqs. (11) and (12), indicating the release of Si and Al and the formation of MgO (Wolbach et al., 1997), which can promote pozzolanic hydration and carbonation reactions:

$$SiO_2 + 2Mg = Si + 2MgO \quad (11)$$

$$Al_2O_3 + 3Mg = 3MgO + 2Al \quad (12)$$

These reactions potentially contributed to the strength enhancement of the GGBS samples by leveraging the activation properties of MgO and the dissolved species to generate dense and hardened $Ca(OH)_2$ and C–S–H gels (Fig. 17).

Fig. 20 shows that the higher rMgO content in the plain rMgO sample (M15) resulted in the rapid formation of expansive hydration products (Table 5), coating the surface of the rMgO particles and decreasing the diffusion of CO_2 gas into the sample, thus reducing the pores and hindering further contact between CO_2 and rMgO. Incorporating SCMs mitigated this negative effect and minimized micro-crack formation during prolonged high-pressure carbonation. rMgO replacement with 5 wt% biochar modified the particle packing in the samples by creating channels for CO_2 diffusion (Fig. 16). This enabled increased reaction between CO_2 and rMgO particles, effectively utilizing rMgO while sequestering CO_2 and improving the strength of the stabilized soil. Furthermore, rMgO replacement with 5 wt% biochar induced delayed expansion of HMCs due to reduced rMgO content, thus facilitating longer carbonation and the formation of HMCs. Although rMgO replacement with GGBS caused delayed expansion of HMCs due to the reduced rMgO content, the fine particle sizes of GGBS and the

Table 6
Energy coefficients of raw materials (Shillaber et al., 2015; Cai et al., 2020; Chen et al., 2022).

Unit	rMgO	Soil	Biochar	GGBS	Water
Energy (MJ/kg)	5	0.083	0.306	0.721	0.01

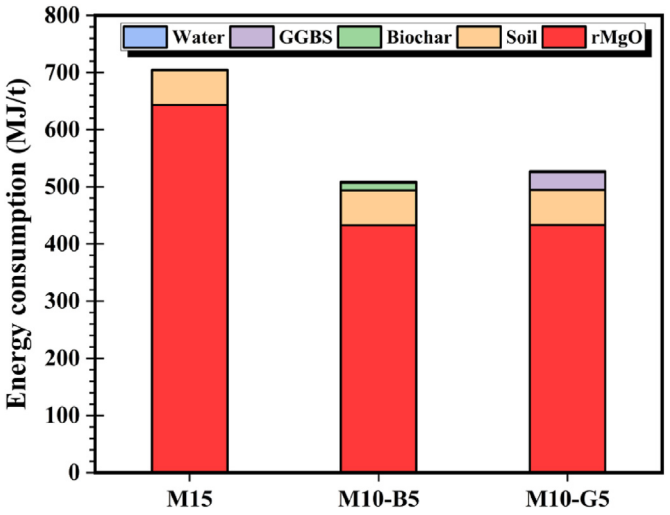

Fig. 19. Energy consumption of raw materials of the stabilized DMS.

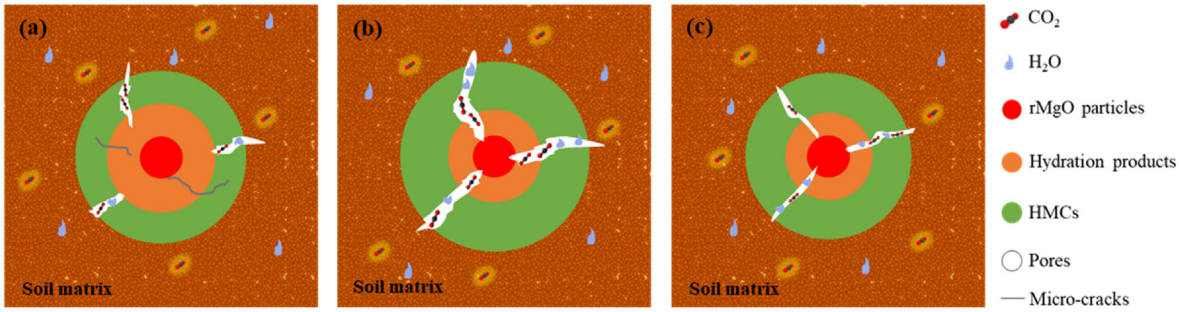

Fig. 20. Schematic illustration of the possible hydration and carbonation phase formation after 6 h of CO_2 curing: (a) rMgO, (b) rMgO-biochar, and (c) rMgO-GGBS.

precipitated hydration products reduced the pores, limiting CO_2 inflow and depriving the system of sufficient CO_2 to react with the rMgO, consequently producing lesser HMCs compared to the biochar samples. Based on the findings, rMgO replacement with 5 wt% biochar led to higher CO_2 uptake, lower energy consumption, and reduced toxicity compared to the plain rMgO or rMgO-GGBS samples. Therefore, biochar can be considered a more environmentally friendly SCM for soil stabilization than GGBS under CO_2 curing.

5. Conclusions

This study assessed the mechanical performance, CO_2 uptake, microstructural properties, and environmental impacts of rMgO-stabilized dredged marine soil containing SCMs. The main findings are summarized as follows:

(1) rMgO replacement with SCMs (i.e. biochar or GGBS) altered the engineering properties and particle packing of the samples, consequently influencing their performance. Biochar samples exhibited higher liquid limits, void ratios, and porosities compared to GGBS samples. The GGBS samples benefited from the high alkaline environment, which promoted pozzolanic reactions to form dense $Ca(OH)_2$ and C—S—H products, leading to improved strength.
(2) Incorporating biochar improved the carbonation efficiency and ductility of the samples, but its large particle sizes and brittleness may weaken the strength. High GGBS content improved strength but impaired the carbonation efficiency. Hence, in view of comprehensive performance, 5 wt% rMgO replacement with biochar or GGBS is recommended for adequate strength and CO_2 uptake.
(3) Replacing rMgO with SCMs delayed the formation of expansive hydration products. The SCMs improved the water-retention capacity, gradually releasing water required for hydration and carbonation reactions, thereby mitigating micro-cracks and shrinkage during long-period high-pressure carbonation.
(4) The nesquehonite, hydromagnesite/dypingite, and calcite products formed in the carbonated samples had higher cementation effects than brucite and other hydration products formed in the ambient cured samples.
(5) MgO-SCMs samples demonstrated reduced global warming potential, and the environmental impact assessment and energy demand analysis indicated that biochar samples are more environment-friendly.
(6) The reaction mechanism suggests that the pozzolans in soil, biochar, and GGBS play a significant role in modifying the pH of the samples, consequently affecting the overall hydration and carbonation process.

Finally, exploring the impact of varying gas pressures and water contents on rMgO-SCMs stabilized DMS presents an intriguing area for future research. Additionally, to advance the current understanding of sustainable production methods, it is recommended that future studies investigate the efficacy of carbonated MgO derived from magnesium silicate minerals. Notably, using energy-efficient techniques in this process offers the additional advantage of zero CO_2 emissions.

Declaration of competing interest

The authors declare that they have no known competing financial interests or personal relationships that could have appeared to influence the work reported in this paper.

Acknowledgments

This work was supported by the Creative Groups of Natural Science Foundation of Hubei Province (Grant No. 2021CFA030). Onyekwena Chikezie Chimere is an awardee for the ANSO Scholarship 2020-PhD. Ishrat Hameed Alvi is a recipient of the 2021 PhD ANSO Scholarship.

Appendix A. Supplementary data

Supplementary data to this article can be found online at https://doi.org/10.1016/j.jrmge.2023.05.005.

References

Akula, P., Little, D.N., 2020. Analytical tests to evaluate pozzolanic reaction in lime stabilized soils. MethodsX 7, 100928.
Al-Tabbaa, A., 2013. Reactive magnesia cement. In: Pacheco-Torgal, F., Jalali, S., Labrincha, J., John, V.M. (Eds.), Eco-Efficient Concrete. Woodhead Publishing, pp. 523–543.
Alvi, I.H., Li, Q., Hou, Y., Onyekwena, C.C., Zhang, M., Ghaffar, A., 2023. A critical review of cement composites containing recycled aggregates with graphene oxide nanomaterials. J. Build. Eng. 69, 105989.
ASTM D2487–11, 2011. Standard Practice for Classification of Soils for Engineering Purposes (Unified Soil Classification System) 1. ASTM International, West Conshohocken, PA, USA.
ASTM D4219-08, 2008. Standard Test Method for Unconfined Compressive Strength Index of Chemical-Grouted Soils. ASTM International, West Conshohocken, PA, USA.
ASTM D4609-08, 2008. Standard Guide for Evaluating Effectiveness of Admixtures for Soil Stabilization. ASTM International, West Conshohocken, PA, USA.
ASTM D854-10, 2010. Standard Test Methods for Specific Gravity of Soil Solids by Water Pycnometer. ASTM International, West Conshohocken, PA, USA.
Cai, G.H., Liu, S.Y., Cao, J.J., Du, G.Y., Wang, N.P., 2016. Influence of the initial water content on the engineering properties of carbonated soil admixed with reactive MgO. In: Geo-Chicago 2016. Sustainable Geoenvironmental Systems, Chicago, pp. 797–806.
Cai, G.H., Liu, S.Y., 2017. Compaction and mechanical characteristics and stabilization mechanism of carbonated reactive MgO-stabilized silt. KSCE J. Civ. Eng. 21 (7), 2641–2654.

Cai, G.H., Liu, S.Y., Du, G.Y., Wang, L., Li, J.S., Liu, L., 2020. Hydraulic conductivity characteristics of carbonated reactive magnesia-treated silt. Bull. Eng. Geol. Environ. 79 (6), 3033–3047.
Cai, G., Liu, S., Du, G., Chen, Z., Zheng, X., Li, J., 2021. Mechanical performances and microstructural characteristics of reactive MgO-carbonated silt subjected to freezing-thawing cycles. J. Rock Mech. Geotech. Eng. 13 (4), 875–884.
Chan, C.M., Abdul Jalil, A.N., 2014. Some insights to the reuse of dredged marine soils by admixing with activated steel slag. Adv. Civ. Eng. 1–7, 2014.
Chen, T., Zhao, L., Gao, X., Li, L., Qin, L., 2022. Modification of carbonation-cured cement mortar using biochar and its environmental evaluation. Cem. Concr. Compos. 134, 104764.
Choudhary, M.P., Charan, H.D., Acharya, B., 2021. Experimental investigation on biochar production and application: solution to air pollution due to stubble burning as well as amending soil consistency. J. Inst. Eng. Ser. A 102 (3), 705–712.
Dissanayake, P.D., Choi, S.W., Igalavithana, A.D., Yang, X., Tsang, D.C.W., Wang, C.H., Kua, H.W., Lee, K.B., Ok, Y.S., 2020. Sustainable gasification biochar as a high efficiency adsorbent for CO_2 capture: a facile method to designer biochar fabrication. Renew. Sustain. Energy Rev. 124, 109785.
Du, Y.J., Wei, M.L., Jin, F., Liu, Z. Bin, 2013. Stress–strain relation and strength characteristics of cement treated zinc-contaminated clay. Eng. Geol. 167, 20–26.
Dung, N.T., Unluer, C., 2017. Sequestration of CO_2 in reactive MgO cement-based mixes with enhanced hydration mechanisms. Construct. Build. Mater. 143, 71–82.
Dung, N.T., Unluer, C., 2020. Influence of accelerated hydration and carbonation on the performance of reactive magnesium oxide concrete. Adv. Cement Res. 32 (2), 78–90.
El-Hassan, H., Shao, Y., Ghouleh, Z., 2013. Reaction products in carbonation-cured lightweight concrete. J. Mater. Civ. Eng. 25 (6), 799–809.
Estabragh, A.R., Jahani, A., Javadi, A.A., Babalar, M., 2020. Assessment of different agents for stabilisation of a clay soil. Int. J. Pavement Eng. 23 (2), 160–170.
Eyo, E.U., Ng'ambi, S., Abbey, S.J., 2020. Incorporation of a nanotechnology-based additive in cementitious products for clay stabilisation. J. Rock Mech. Geotech. Eng. 12 (5), 1056–1069.
Fasihnikoutalab, M.H., Pourakbar, S., Ball, R.J., Huat, B.K., 2017. The effect of olivine content and curing time on the strength of treated soil in presence of potassium hydroxide. Int. J. Geosynth. Gr. Eng. 3 (2), 1–10.
Geeta Rani, T., Tulasi, K., Sai Rama Krishna, Y., 2017. Ground granulated blast furnace slag as an expansive soil stabilizer. VFSTR J. STEM 3 (1), 2455–2062.
Gonzalez, J., Sargent, P., Ennis, C., 2021. Sewage treatment sludge biochar activated blast furnace slag as a low carbon binder for soft soil stabilisation. J. Clean. Prod. 311, 127553.
Gross, J., Adaska, W., 2020. Guide to Cement-Stabilized Subgrade Soils. Iowa State University, National Concrete Pavement Technology Center.PCA Special Report SR1007P. https://intrans.iastate.edu/app/uploads/2020/05/guide_to_CSS.pdf.
Grünhäuser Soares, E., Castro-Gomes, J., 2021. Carbonation curing influencing factors of carbonated reactive magnesia cements (CRMC) – a review. J. Clean. Prod. 305 (7), 127210.
Gupta, S., 2021. Carbon sequestration in cementitious matrix containing pyrogenic carbon from waste biomass: a comparison of external and internal carbonation approach. J. Build. Eng. 43, 102910.
Han, X., Jiang, N., Jin, F., Reddy, K.R., Wang, Y., Liu, K., Du, Y., 2022. Effects of biochar-amended alkali-activated slag on the stabilization of coral sand in coastal areas. J. Rock Mech. Geotech. Eng. 15 (3), 760–772.
Hay, R., Celik, K., 2020. Hydration, carbonation, strength development and corrosion resistance of reactive MgO cement-based composites. Cement Concr. Res. 128, 105941.
He, S., Chen, G., Xiao, H., Shi, G., Ruan, C., Ma, Y., Dai, H., Yuan, B., Chen, X., Yang, X., 2021. Facile preparation of N-doped activated carbon produced from rice husk for CO_2 capture. J. Colloid Interface Sci. 582, 90–101. https://doi.org/10.1016/J.JCIS.2020.08.021.
Kara, S., Erdem, S., Lezcano, R.A.G., 2021. MgO-based cementitious composites for sustainable and energy efficient building design. Sustain. Times 13 (16), 9188.
Lang, L., Chen, Bowen, Chen, Bing, 2021a. Strength evolutions of varying water content-dredged sludge stabilized with alkali-activated ground granulated blast-furnace slag. Construct. Build. Mater. 275, 122111.
Lang, L., Chen, B., Duan, H., 2021b. Modification of nanoparticles for the strength enhancing of cement-stabilized dredged sludge. J. Rock Mech. Geotech. Eng. 13 (3), 694–704.
Li, J.S., Zhou, Y., Chen, X., Wang, Q., Xue, Q., Tsang, D.C.W., Poon, C.S., 2021. Engineering and microstructure properties of contaminated marine sediments solidified by high content of incinerated sewage sludge ash. J. Rock Mech. Geotech. Eng. 13 (3), 643–652.
Li, W., Qin, J., Yi, Y., 2021. Carbonating MgO for treatment of manganese- and cadmium-contaminated soils. Chemosphere 263, 128311.
Li, W., Qin, J., Yi, Y., 2022a. Treating Pb-contaminated clay slurry by three curing agents. Chemosphere 303, 135011.
Li, W., Yi, Y., Puppala, A.J., 2022b. Comparing carbide sludge-ground granulated blastfurnace slag and ordinary Portland cement: different findings from binder paste and stabilized clay slurry. Construct. Build. Mater. 321, 126382.
Liu, S.Y., Cai, G.H., Cao, J., Wang, F., 2020. Influence of soil type on strength and microstructure of carbonated reactive magnesia-treated soil. Eur. J. Environ. Civ. Eng. 24 (2), 248–266.
Liu, Z., Meng, W., 2021. Fundamental understanding of carbonation curing and durability of carbonation-cured cement-based composites: a review. J. CO_2 Util. 44, 101428.
Ma, W., Yi, Y., Fang, M., Li, C., Li, J., Liu, W., 2023. Study on the synthesis mechanism of sodalite, gismondine, and zeolite-P1 zeolite materials from ladle furnace slag and fly ash. Sci. Rep. 13 (1), 3232.
Ma, Z., Han, S., 1987. The refinement of crystal structure of balipholite. Sci. Sin. 7, 780–784.
Manzoor, S.O., Yousuf, A., 2020. Stabilisation of soils with lime: a Review. J. Mater. andEnvironmental Sci. 11 (9), 1538–1551.
Mo, L., Zhang, F., Panesar, D.K., Deng, M., 2017. Development of low-carbon cementitious materials via carbonating Portland cement–fly ash–magnesia blends under various curing scenarios: a comparative study. J. Clean. Prod. 163, 252–261.
Noolu, V., Mallikarjuna Rao, G., Sudheer Kumar Reddy, B., Chavali, R.V.P., 2021. Strength and durability characteristics of GGBS geopolymer stabilized black cotton soil. Mater. Today Proc. 43, 2373–2376.
Onyekwena, C.C., Li, Q., Alvi, I.H., Ghaffar, A., Zhang, X., 2023a. Geomechanical performances of geocell reinforced retaining wall backfilled with magnesia-based cement stabilized marine fill. Mar. Georesour. Geotechnol. 1–17.
Onyekwena, C.C., Xue, Q., Li, Q., Umeobi, H.I., Ghaffar, A., Fasihnikoutalab, M.H., 2023b. Advances in the carbonation of MgO-based binder and CO_2 utilization in the construction industryAdvances in the carbonation of MgO-based binder and CO_2 utilization in the construction industry. Clean Technol. Environ. Policy. https://doi.org/10.1007/s10098-023-02482-7.
Onyekwena, C.C., Xue, Q., Li, Q., Wan, Y., Feng, S., Umeobi, H.I., Liu, H., Chen, B., 2022. Support vector machine regression to predict gas diffusion coefficient of biochar-amended soil. Appl. Soft Comput. 127, 109345.
Pardo, G.S., Sarmah, A.K., Orense, R.P., 2019. Mechanism of improvement of biochar on shear strength and liquefaction resistance of sand. Geotechnique 69 (6), 471–480.
Pu, L., Unluer, C., 2020. Effect of preconditioning on carbonated reactive MgO-based concrete samples. J. Mater. Civ. Eng. 32 (11), 04020314.
Reddy, K.R., Yargicoglu, E.N., Chetri, J.K., 2020. Effects of biochar on methane oxidation and properties of landfill cover soil: long-term column incubation tests. J. Environ. Eng. 147 (1), 04020144.
Ruan, S., Unluer, C., 2017. Influence of mix design on the carbonation, mechanical properties and microstructure of reactive MgO cement-based concrete. Cem. Concr. Compos. 80, 104–114.
Ruan, S., Liang, S., Kastiukas, G., Zhu, W., Zhou, X., 2020. Solidification of waste excavation clay using reactive magnesia, quicklime, sodium carbonate and early-age oven curing. Construct. Build. Mater. 258, 120333.
Ruan, S., Wang, T., Guo, R., Unluer, C., 2021. Assessment of the properties and environmental impact of carbonated reactive magnesia containing industrial waste. Thermochim. Acta 706, 179051.
Sethupathi, S., Zhang, M., Rajapaksha, A.U., Lee, S.R., Nor, N.M., Mohamed, A.R., Al-Wabel, M., Lee, S.S., Ok, Y.S., 2017. Biochars as potential adsorbers of CH_4, CO_2 and H_2S. Sustain. Times 9 (1), 121.
Sharma, A.K., Sivapullaiah, P.V., 2016. Ground granulated blast furnace slag amended fly ash as an expansive soil stabilizer. Soils Found. 56 (2), 205–212.
Sharma, M., Satyam, N., Reddy, K.R., 2021. Rock-like behavior of biocemented sand treated under non-sterile environment and various treatment conditions. J. Rock Mech. Geotech. Eng. 13 (3), 705–716.
Shen, W., Cao, L., Li, Q., Wen, Z., Wang, J., Liu, Y., Dong, R., Tan, Y., Chen, R., 2016. Is magnesia cement low carbon? Life cycle carbon footprint comparing with Portland cement. J. Clean. Prod. 131, 20–27.
Shi, W., Chen, Q., Nimbalkar, S., Liu, W., 2017. A new mixing technique for solidifier and dredged fill in coastal area. Mar. Georesour. Geotechnol. 35 (1), 52–61.
Shillaber, C.M., Mitchell, J.K., Dove, J.E., 2015. Energy and carbon assessment of ground improvement works. II: working model and example. J. Geotech. Geoenviron. Eng. 142 (3), 04015084.
Unluer, C., 2018. Carbon dioxide sequestration in magnesium-based binders. In: Pacheco-Torgal, F., Shi, C., Palomo, A. (Eds.), Carbon Dioxide Sequestration in Cementitious Construction Materials. Elsevier, pp. 129–173.
Wang, D., Zentar, R., Abriak, N.E., 2016. Temperature-accelerated strength development in stabilized marine soils as road construction materials. J. Mater. Civ. Eng. 29 (5), 04016281.
Wang, D., Zhu, J., He, F., 2019a. Quantification and micro-mechanisms of CO_2 sequestration in magnesia-lime-fly ash/slag solidified soils. Int. J. Greenh. Gas Control 91, 102827.
Wang, D., Zhu, J., He, F., 2019b. CO_2 carbonation-induced improvement in strength and microstructure of reactive MgO-CaO-fly ash-solidified soils. Construct. Build. Mater. 229, 116914.
Wang, F., Shen, Z., Liu, R., Zhang, Y., Xu, J., Al-Tabbaa, A., 2020. GMCs stabilized/solidified Pb/Zn contaminated soil under different curing temperature: physical and microstructural properties. Chemosphere 239, 124738.
Wang, L., Chen, L., Poon, C.S., Wang, C.H., Ok, Y.S., Mechtcherine, V., Tsang, D.C.W., 2021. Roles of biochar and CO_2 curing in sustainable magnesia cement-based composites. ACS Sustain. Chem. Eng. 9 (25), 8603–8610.
Wolbach, W.S., Bryan, S.R., Shoemaker, G.L., Krucek, T.W., Maier, R.D., Soni, K.K., Chabala, J.M., Mogilevsky, R., Levi-Setti, R., 1997. Optimization of chemical reactions between alumina/silica fibres and aluminium-magnesium alloys during composite processing. J. Mater. Sci. 32 (8), 1953–1961.

Wu, H.L., Zhang, D., Ellis, B.R., Li, V.C., 2018. Development of reactive MgO-based engineered cementitious composite (ECC) through accelerated carbonation curing. Construct. Build. Mater. 191, 23–31.
Wu, J., Liu, L., Deng, Y., Zhang, G., Zhou, A., Xiao, H., 2022. Use of recycled gypsum in the cement-based stabilization of very soft clays and its micro-mechanism. J. Rock Mech. Geotech. Eng. 14 (3), 909–921.
Yaghoubi, M., Arulrajah, A., Disfani, M.M., Horpibulsuk, S., Bo, M.W., Darmawan, S., 2018. Effects of industrial by-product based geopolymers on the strength development of a soft soil. Soils Found. 58 (3), 716–728.
Yi, Y., Liska, M., Akinyugha, A., Unluer, C., Al-Tabbaa, A., 2013. Preliminary laboratory-scale model auger installation and testing of carbonated soil-MgO columns. Geotech. Test J. 36 (3), 1–10.
Yi, Yaolin, Liska, M., Al-Tabbaa, A., 2014. Properties of two model soils stabilized with different blends and contents of GGBS, MgO, lime, and PC. J. Mater. Civ. Eng. 26 (2), 267–274.
Yi, Y., Lu, K., Liu, S.Y., Al-Tabbaa, A., 2016. Property changes of reactive magnesia–stabilized soil subjected to forced carbonation. Can. Geotech. J. 53 (2), 314–325.
Yu, C., Cui, C., Zhao, J., Zheng, J., 2021. A novel approach to utilizing dredged materials at the laboratory scale. Construct. Build. Mater. 313, 125568.
Zhang, W. lu, Zhao, L. yang, McCabe, B.A., Chen, Y. hui, Morrison, L., 2020. Dredged marine sediments stabilized/solidified with cement and GGBS: factors affecting mechanical behaviour and leachability. Sci. Total Environ. 733, 138551.
Zhang, Y., Gu, K., Tang, C., Shen, Z., Narala, G.R., Shi, B., 2020. Effects of biochar on the compression and swelling characteristics of clayey soils. Int. J. Geosynth. Ground. Eng. 6 (2), 1–8.
Zhang, Y., Ong, Y.J., Yi, Y., 2022. Comparison between CaO- and MgO-activated ground granulated blast-furnace slag (GGBS) for stabilization/solidification of Zn-contaminated clay slurry. Chemosphere 286, 131860.
Zhao, Y., Li, Y., Fan, D., Song, J., Yang, F., 2021. Application of kernel extreme learning machine and Kriging model in prediction of heavy metals removal by biochar. Bioresour. Technol. 329, 124876.
Zhu, J.F., Xu, R.Q., Zhao, H.Y., Luo, Z.Y., Pan, B.J., Rao, C.Y., 2020. Fundamental mechanical behavior of CMMOSC-S-C composite stabilized marine soft clay. Appl. Clay Sci. 192, 105635.

Chikezie Chimere Onyekwena is a Civil Engineer specializing in Geotechnical Engineering. He holds a Ph.D. in Geotechnical Engineering from the Institute of Rock and Soil Mechanics, Chinese Academy of Sciences. He is an active member of the American Society of Civil Engineers (ASCE) and currently serves as a reviewer for various international journals. His research interests include flow through porous media and the stabilization of soft soils, with a focus on developing innovative, low-carbon, and functional construction products with high performance and durability. He is also experienced in using AI tools for advanced engineering computations.